A Novel Dynamic Model to Estimate the Reactivity Ratios of Ethylene/1-Olefin Copolymers

by

Salman Obaidoon

A thesis submitted in partial fulfillment of the requirements for the degree of

Master of Science

in

Chemical Engineering

Department of Chemical and Materials Engineering

University of Alberta

Abstract

Polyolefins are the largest class of commodity polymers. Polyethylene and polypropylene are the most common commercial types of these polymers. The former accounts for nearly one-third of the world polymer market and it is predicted that its demand will keep growing in the foreseeable future. Commercial polyethylene resins are produced as homopolymers or copolymers of ethylene with α-olefins.

Polymerization kinetic models are needed to predict the microstructures and properties of polyolefins. These models contain unknown parameters whose values are sometimes difficult to estimate; reactivity ratios are among them. A method that is widely used to estimate reactivity ratios is to perform low-conversion copolymerizations at several initial monomer feed compositions. Reactivity ratio estimates are obtained by fitting the copolymer composition data made at several comonomer ratios to a suitable form of the copolymer composition equation (the Mayo-Lewis equation) through linear or non-linear regression. Sometimes, significant composition drift occurs during the polymerizations, requiring an alternative approach using dynamic modeling and optimization.

In this thesis, the microstructural characteristics, including reactivity ratios, of ethylene/1-hexene and ethylene/1-octene copolymers made with constrained geometry catalysts (CGC) were investigated in a semi-batch reactor. The catalyst was activated with modified methylaluminoxane (MMAO) or with dimetylanilinium tetrakis (pentafluorophenyl) borate. The investigation was based on the effect of comonomer concentration and polymerization time on the copolymer properties.

To estimate the reactivity ratios of these copolymers, a dynamic mathematical model was developed, combining the Mayo-Lewis equation and phase equilibrium calculations. The method can be applied to two cases: 1) only one polymerization is done and samples are taken from the reactor at different polymerization times, or 2) a set of polymerization runs are done with the same feed composition and operation conditions, but at different polymerization times. The model generates ordinary differential equations for each polymerization mode. The simultaneous numerical solution of the differential equations for all polymerization runs provides reliable

estimates of the reactivity ratios. It also predicts the molar fractions of comonomer in the reactor as a function of time for all polymerizations using the estimated values.

Acknowledgements

I would like to express my sincere gratitude to many people around me who made this work possible. First, I am grateful to my thesis supervisor Prof. João B.P. Soares for believing in me from the early beginnings and allowing me to grow and flourish. Not only his guidance and immense knowledge that supported me but also his perspective on life and research that I will carry for the rest of my life.

I would like to thank Dr. Saied Mehdiabadi for his coaching, support, and insightful thoughts and discussions throughout my project. I am grateful for the opportunity to get to know him as a person and a scientist who's always ready to help and share his knowledge.

I would like to express my gratitude to Hadhramout Foundation for sponsoring my MSc program.

Special thanks to Dr. Adriano Fisch, Mrs. Linda Kaert, and my colleagues Venugopal Hegde and Raunil Raj for their support, assistance, and inspiration.

My deepest gratitude to my parents for all the sacrifices, inspiration, and unconditional love they gave me. Without it, I might not be the person I am today. I would also like to acknowledge my gratitude and thanks to my fiancée and love Mary Al-Hadhrami for her patience, support, understanding, and always being there for me.

Table of Contents

List of Tables

List of Figures

Chapter 1: Introduction

1.1 Motivation and Objectives

Polyolefins are a dominant class of synthetic polymers that are produced by the polymerization of olefins such as ethylene, propylene, 1-butene, and higher 1-olefins as homopolymers (single olefin monomers) or copolymers (multi olefins monomers). The market growth (5-6% per year) shows the significance of this commodity in everyday life. This growth is attributed to their excellent physical and mechanical properties, low production cost, raw materials availability, and the versatility of its applications.[1] Examples of polyolefins applications include, but are not limited to, food packaging, toy manufacturing, home and medical appliance, automotive parts, and sports items. [2]

Commercial polyolefins have experienced crucial changes over the last six decades starting in the early 1930s when two British scientists working at the Imperial Chemical Industries (ICI) accidentally produced polyethylene (PE) during high-pressure experiments of ethylene with different compounds.[3] Following that serendipitous discovery, major developments have occurred leading to the commercial processes known today. Figure 1.1.[4] shows the historical stages of these developments, passing through various breakthrough discoveries that attempted to improve the polymer microstructure and performance.

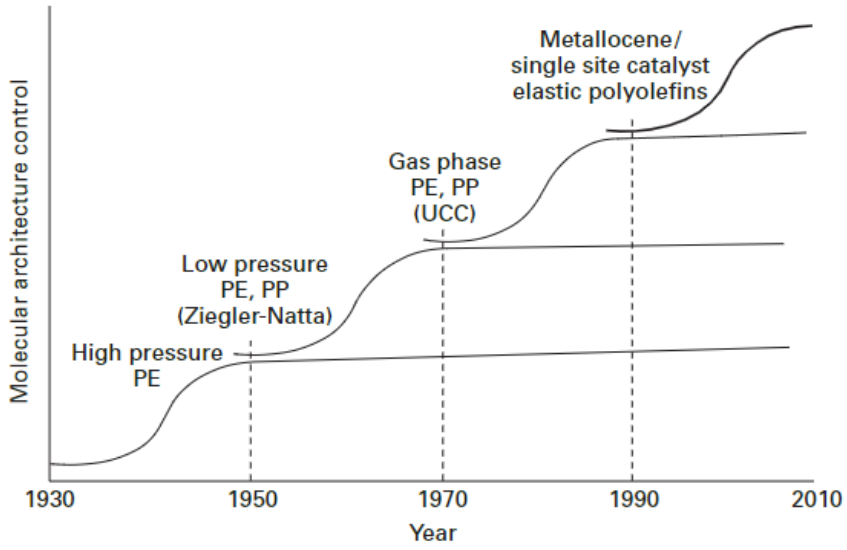

Figure 1.1 Historical developments of polyolefins catalysts and polymerization processes.

Polyolefins can be categorized into two main types, polyethylene (PE) and polypropylene (PP), which comprise about 60% of the global plastics market.[5,6] Polyethylenes of different types—low-density polyethylene (LDPE), linear low-density polyethylene (LLDPE), and high-density polyethylene (HDPE)—share 36% of that market percentage. Three microstructural distributions—molecular weight distribution (MWD), chemical composition distribution (CCD), also known as short chain branching, and long chain branching (LCB)—determine the properties of these polyethylene grades.[7] The breadth of PE microstructural distributions results from the different processes applied to produce these resins. LDPE is made using free radical polymerization under high pressure and contains both short chain branching (SCB) and LCB, while LLDPE and HDPE are synthesized with coordination polymerization and have only SCBs.[8]

Coordination polymerizations, regardless of the type of catalyst used, need a catalyst precursor, activator (cocatalyst), and monomers (ethylene, propylene, longer α-olefins).[9] The concentration of reagents and temperature at the active sites control the polymerization kinetics of these systems. Mathematical models are used to describe the behavior of polymerizations and predict polymer microstructures and properties. These models contain unknown parameters whose values are often difficult to estimate: reactivity ratios are among them.

The objectives of this thesis are: 1) to develop a dynamic mathematical model that combines the Mayo-Lewis equation and phase equilibrium calculations to estimate the reactivity ratios of ethylene/1-hexene copolymers with two catalytic systems, CGC/MMAO and CGC/B/TOA, and 2) to perform the same calculations for ethylene/1-octene copolymers.

1.2 Thesis Outline

This thesis consists of six chapters

Chapter 1: A brief overview of the research project including the research objectives and the thesis outline.

Chapter 2: Literature review of polyethylene resins, their polymerization catalysts and processes, and methods to estimate reactivity ratios.

Chapter 3: Description of polymerization procedures and characterization techniques.

Chapter 4: Estimation of reactivity ratios for the copolymerization of ethylene and 1-hexene with CGC/MMAO and CGC/B/TOA.

Chapter 5: Estimation of reactivity ratios for the copolymerization of ethylene and 1-octene with CGC/MMAO.

Chapter 6: Conclusions and recommendations for future work.

1.3 Literature Review

1.3.1 Polyethylene

Polyethylene resins can be divided into three types: low-density polyethylene (LDPE), linear low-density polyethylene (LLDPE), and high-density polyethylene (HDPE). As their names imply, they are classified according to their density range. Although polymer molecular weight affects density slightly, it is most influenced by short chain branching (SCB). Figure 1.2 illustrates how these polymers are classified according to their microstructures.[10]

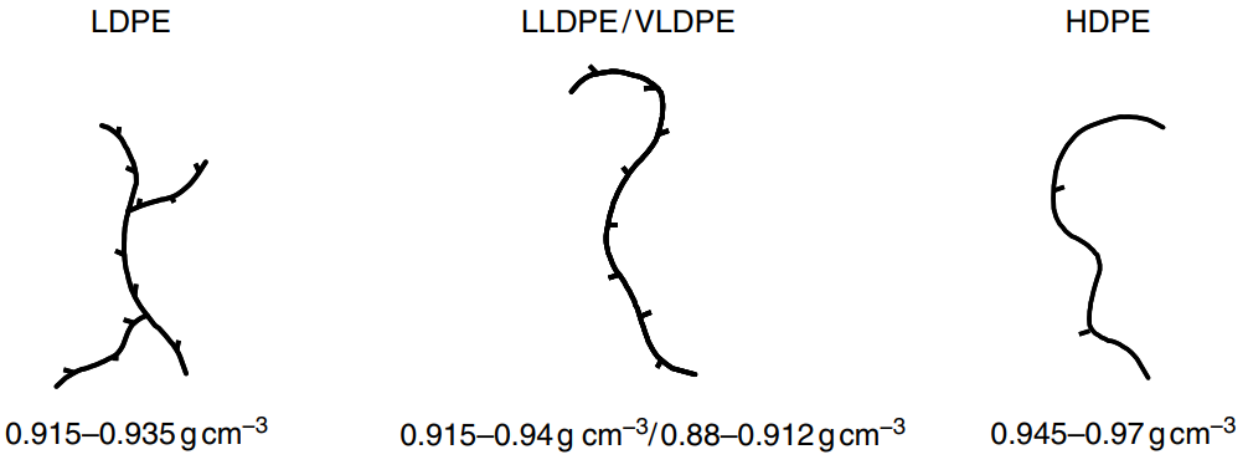

Figure 1.2 Classification of polyethylenes based on branching structure and density.

LDPE is produced using autoclaves or tubular reactors under high pressure (> 500 atm) and temperature (> 100 °C) in the presence of oxygen traces (0.01 – 5) wt% that form free radical

initiators.[11] These resins have LCBs and SCBs. The latter are formed via backbiting reactions—as much as 20 to 30 per 1000 C atoms—while the former results from chain transfer to polymer—about 10 SCBs per LCB.[11–14] HDPE and LLDPE are made with organometallic coordination catalysts under much lower temperature and pressure; their SCBs are made by copolymerizing ethylene and α-olefins. HDPE was first produced by Karl Ziegler using a aluminum alkyl/titanium halide catalytic system. Its high density (greater than 0.94 g cm^{-3}) is attributed to the low molar fraction of α-olefin in the polymer chains, providing higher stiffness, processability, and excellent chemical resistance to these polymers.

Since HDPE is not suitable to make many flexible packaging applications, the doors were opened to another polyethylene type that could match the LDPE properties and could be made under low temperature and pressure: the LLDPE resins. The same polymerization system used to make HDPE was applied to synthesize LLDPE, which was first commercialized by DuPont in the early 1960s.[11] The term "linear" stems from the fact that no LCBs are present in these resins (differently from the similar density LDPE resins). They differ from HDPE mostly because of the higher fraction of α-olefin incorporated in the polymer chains.

1.3.2 Polyethylene Polymerization Catalysts

The evolution of commercial polyethylene started in the early 1950s with the breakthrough discovery of coordination catalysts by Karl Ziegler and Giuseppe Natta. Before that, free radical initiators were used as activators for PE synthesis.[15] Coordination complexes capitalize on the catalytic nature of transition metal atoms. Four groups of catalysts have been derived from this general idea: Ziegler-Natta, chromium oxide (Phillips), metallocene, and late transition metal (post-metallocene) catalysts.

1.3.2.1 Ziegler-Natta Catalysts

Ziegler-Natta catalysts consist of two components: a transition metal salt from groups IV to VII, such as $TiCl_3$ and $TiCl_4$ (pre-catalysts) and a metal cation from groups I to III (cocatalyst). The metal alkyl cocatalysts—preferably aluminum alkyls such as $Al(C_2H_5)$—activate the transition metal centers through alkylation and reduction.[2] Depending on the state of the complex in the

polymerization medium, they can be sub-divided into homogeneous or heterogeneous catalysts. The former is mostly associated with vanadium-based catalysts that are soluble in the reaction medium. They have a single type of active site, making polyolefins with uniform microstructures (narrow MWDs and CCDs) such as ethylene-propylene-diene (EPDM) elastomers. Contrarily, heterogeneous Ziegler-Natta catalysts are insoluble in the reaction medium and have more than one type of active site, making polyethylenes with nonuniform molecular architectures, with broad and sometimes bimodal MWDs and CCDs. They are used to synthesize different grades of polyethylenes at mild polymerization conditions. $TiCl_4$ supported on $MgCl_2$ or SiO_2 are the most common types of Ziegler-Natta catalysts, providing high catalytic activity and better control of the active sites.[16,17] (Figure 1.3)

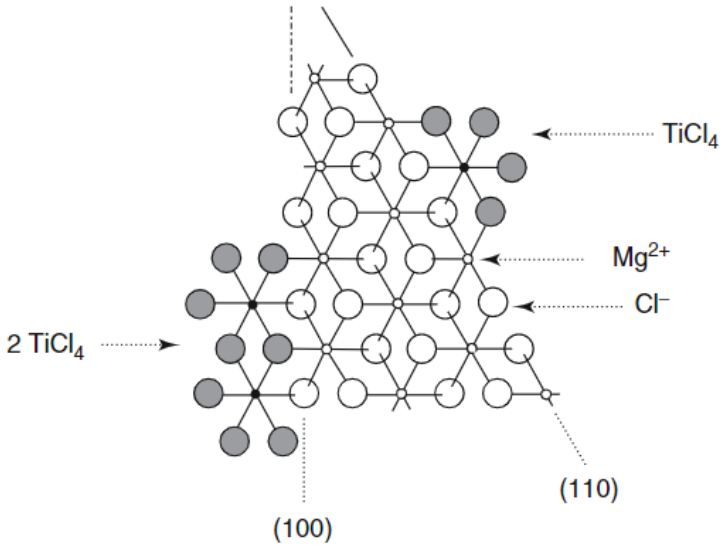

Figure 1.3 Structure of $TiCl_4/MgCl_2$ Ziegler-Natta catalyst.[2]

1.3.2.2 Phillips Catalysts

Phillips catalysts were developed by Paul Hogan in the early 1950s at the Phillips Petroleum Company. Their complexes consist of chromium oxide (CrO_3) supported on silica (SiO_2) and alumina particles.[18] Like heterogeneous Ziegler-Natta catalysts, they have more than one type of active site and make HDPE with nonuniform microstructure and broad MWD and CCD. These catalysts do not need aluminum alkyls or any other cocatalysts used with Ziegler-Natta catalysts,

as they get activated through a calcination process in dry air at high temperatures. This process affects the catalyst activity and the polymer microstructural properties. Interestingly, these catalysts are not suitable for LLDPE production due to the low tendency of α-olefins incorporation in the polymer chain (low reactivity ratios).[2]

1.3.2.3 Metallocene Catalysts

In the mid-1950s, Natta and Breslow investigated the effect of organic ligands on heterogeneous Ziegler-Natta catalysts using alky aluminum compounds ($AlEt_3$) as activators. Although they used bis-(cyclopentadienyl)-titanium dichloride (Cp_2TiCl_2), this metallocene had an extremely low activity for polyethylene synthesis and failed to polymerize propylene.[19] Metallocenes were deemed inappropriate for commercial applications until the early 1980s, when Kaminsky and Sinn discovered that methylaluminoxane (MAO) could activate and stabilize these catalysts. Later, Exxon Chemical produced the first commercial polyolefin (ethylene-propylene elastomers) using Zr as the transition metal atom (zirconocene catalysts) in 1991.[20] In its broadest definition, a metallocene catalyst is composed of a transition metal atom, such as Zr, Ti, and Hf, sandwiched between two cyclopentadienyl rings that may be connected by bridges of different types. The type of transition metal atom and structure of the ligands (shape, geometry, and chemical nature) affect the catalyst behavior (activity and selectivity). Many metallocene structures can be created by varying the chemical substituents and bridging groups in their structures. Figure 1.4 illustrates the structure of a typical metallocene.

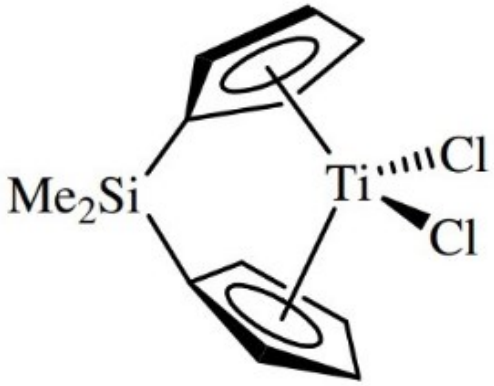

Figure 1.4 Typical structure of a metallocene catalyst.[2]

The unique structure of show in Figure 1.5, containing only one cyclopentadienyl ring, is called "half-sandwich" or constraint geometry catalyst (CGC). Due to their open structure, these catalysts are more stable at high temperatures and have very high reactivity ratios towards α-olefins incorporation, making them a great choice for ethylene/α-olefins copolymerization. There catalysts might also form LCBs via terminal branching—the polymerization of vinyl-terminated polymer chains (macromonomers).[21] This LCBs may have a considerable impact on polymer properties such as increasing shear thinning and processability, as well as enhancing the polymer melt elasticity.[2]

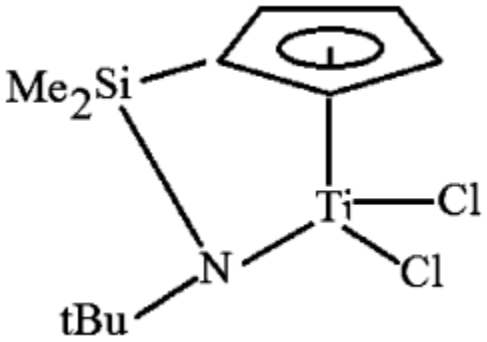

Figure 1.5 Representative structure of a constraint geometry catalyst.[21]

Unsupported metallocenes are soluble in the polymerization medium. They are classified as single-site catalysts because they make polyolefins with uniform microstructures (narrow MWD and CCD). They can also be supported onto different carriers, such as silica or alumina, becoming heterogeneous catalysts that are needed in industrial processes developed to run with heterogeneous Ziegler-Natta or Phillips catalysts.[22]

The discovery of MAO as an effective cocatalyst for metallocenes brought them abruptly into the commercial polyolefin market.[23] MAO is an oligomeric compound produced by the controlled reaction of trimethylaluminum (TMA) and water. Despite its importance, the exact structure of MAO is still being disputed. Figure 1.6 shows some of these proposals, out of many structures reported in the literature. MAO also can be bought as modified MMAO (MMAO), which is prepared by the controlled reaction of water with a mixture of TMA and triisobutylaluminum (TIBA). MMAO is more soluble in aliphatic solvents (commonly used in the industry) than MAO.[24,25]

Another family of cocatalysts suitable for stabilizing previously alkylated metallocenes is perfluoroaryl boron-based activators.[26,27] The most common example of these cocatalysts is dimetylanilinium tetrakis (pentafluorophenyl) borate, $[PhNMe_2H]^+[B(C_6F_5)_4]^-$. One advantage of borate cocatalysts is that they can be used in near stoichiometric proportions with the pre-catalyst, in contrast to MAO that is needed in high excesses.

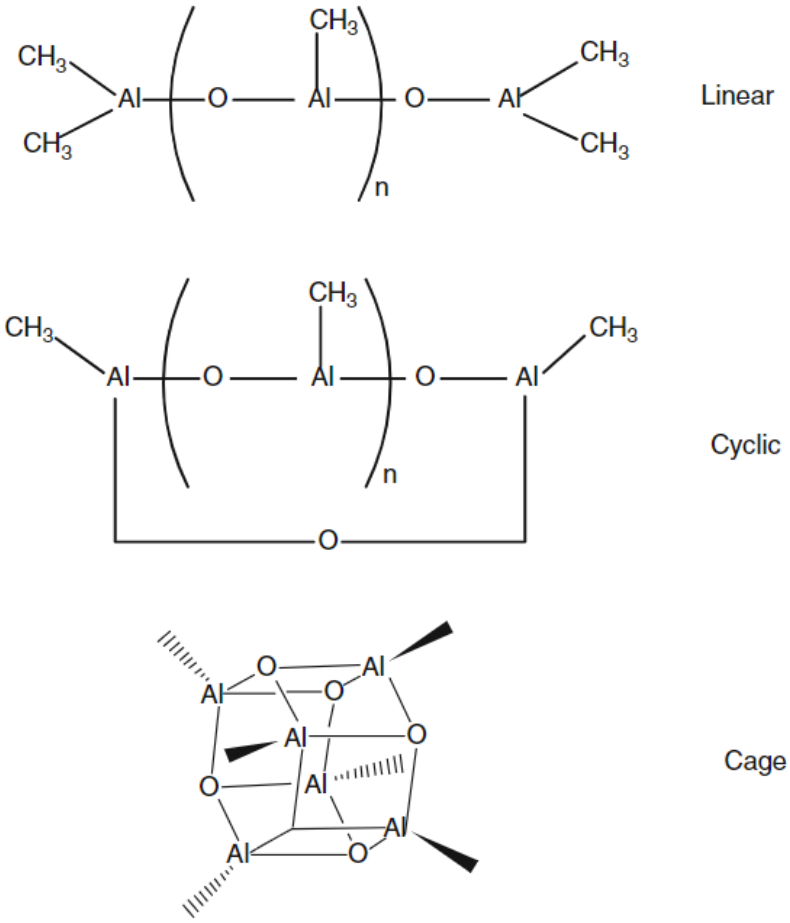

Figure 1.6 Proposed MAO structures.[2]

1.3.2.4 Late Transition Metal Catalysts

Late transition metal catalysts or post-metallocenes are the last group of coordination catalysts that were discovered about one decade after metallocenes. They were first reported by Brookhart and co-workers at DuPont in 1995, making branched polyethylene with high molecular weight in the absence of comonomers.[28] This behavior was attributed to the chain-walking mechanism where

the active site moves along the polymer backbone (via isomerization). When a monomer is inserted in an active site that is not at the chain end and resumes growing the chain, the original chain end becomes a short chain branch. Late transition catalysts have high activity and can produce polyethylene with high molecular weight. They are also more tolerant to polar comonomers, protic impurities, and poisons than other coordination catalysts, making them attractive choices to copolymerize ethylene with polar comonomers such as vinyl alcohols, acrylates, or other vinyl polar comonomers.[29] Despite their unique behavior, these catalysts have yet to meet their commercial potential.

1.3.3 Polyethylene Polymerization Processes

Polyolefins, including polyethylene, can be produced in a wide range of polymerization processes with different coordination catalysts. Polyethylene processes can be classified into solution, slurry, and gas-phase processes. A brief overview of these processes is given below.

1.3.3.1 Solution Polymerization

This is the preferred process for homogeneous metallocenes, since all polymerization components (catalyst, cocatalyst, monomer, and polymer) are soluble in the reaction medium. These processes operate at high temperatures (up to 250 °C) and high pressure (< 100 bar) using one or more reactors: mostly autoclave, but also tubular and loop reactors.[2] The high temperatures guarantee that the polymer is dissolved in the reaction medium. The high temperature along with the absence of mass transfer resistance leads to much higher polymerization rates and shorter residence times—typically 1 to 20 min—compared to gas and slurry processes where average reactor resident times could be as high as 4 hours, providing an advantage for solution processes during grade transition.[30]

1.3.3.2 Slurry Polymerization

Polyethylene is produced commercially in slurry processes with the use of inert diluents (C_3H_8-C_6H_{14}) to suspend the polymer particles while gaseous ethylene is fed into the reactor. These

processes employ heterogeneous catalysts, around which the polymer is formed as a solid swollen in the diluent. Autoclaves or loop reactors are the only two choices for slurry polymerization, which operate under relatively mild conditions. Slurry processes have some advantages over gas-phase reactors, such as better heat transfer capacity and temperature control, as a result of the high heat capacity of the diluent. However, the diluent must be removed and recycled back to the polymerization reactors, adding more operational costs and potentially posing more risk to the environment.[30]

1.3.3.3 Gas-phase Polymerization

Fluidized bed reactors are the only class of reactors used to make polyethylene in the gas phase. In these reactors, the polymer particles are suspended by fluidization in a flow of ethylene, α-olefin comonomer, and nitrogen. The reactors have two operation modes (condensed and dry) with a temperature range of 90-110 °C for the former and 70-90 °C for the dry mode. Since all reactants are present as gases, it is easy to separate them from the polymer by flashing them off the reactor. This reduces production costs and makes it the economically preferred technology for commercial polyethylene production.[2] Another advantage of gas-phase over slurry processes is that they can make polyolefins with lower densities (higher SCB frequencies) that would be extracted by the diluent in slurry process and foul the reactor. However, it is harder to remove heat from the low heat capacity environment in gas-phase reactors, which may lead to runaway polymerizations. Some of the solutions for this problem include the addition of heat transfer agents or setting the inlet gas temperature at the bottom of the reactor below its dew point.[31]

1.3.4 Reactivity Ratio Estimation

Monomer reactivity ratios determine the copolymer structure and the molar fraction of each comonomer in the copolymer (average copolymer composition). The knowledge of these parameters is vital to develop copolymerization kinetics models that describe the copolymer microstructure.[32] Over the years, many techniques have been applied to estimate the reactivity ratios: linear least-squares (LLS) and nonlinear least-squares (NLLS) methods. LLS methods, such as Finemann-Ross (FR), Kelen-Tüdös (KT), extended Kelen-Tüdös (EKT), and Yezrielev-

Brokhina-Roskin (YBR), estimate reactivity ratios using the instantaneous copolymer composition equation, also called the Mayo-Lewis (ML) equation,[33]

$$\frac{F_1}{F_2} = \frac{r_1[M_1]^2 + [M_1][M_2]}{r_2[M_2]^2 + [M_1][M_2]} \tag{2.1}$$

where F_1 and F_2 are the instantaneous mole fraction of monomer 1 and 2 in the copolymer, $r_1 = k_{11}/k_{12}$ and $r_2 = k_{22}/k_{21}$ are the reactivity ratios, $[M_1]$ and $[M_2]$ are the concentration of monomer 1 and 2, respectively. The previous methods, except for EKT, are only applicable at low conversion ($\sim <$ 10%), whereas EKT could account for higher conversions ($\sim <$ 40%).[34,35] Although these methods are easy to compute, they often have drawbacks associated with experimental error and are better used only for initial estimations. On the other hand, NLLS methods estimate reactivity ratios based on the integration of the copolymer composition equation, minimizing the effect of experimental error.[36,37] Tidwell-Mortimore (TM)[38] and other forms of error-in-variables-model (EVM) are some examples of this approach. Some of these methods are briefly reviewed below.

1.3.4.1 Finemann-Ross Method

This is the earliest attempt to linearize the copolymer composition equation, Eq. (2.1), through the transformation proposed below,

$$\frac{f_1(1-2F_1)}{F_1(1-f_1)} = r_1\left[\frac{f_1^2(F_1-1)}{F_1(1-f_1)^2}\right] + r_2 \tag{2.2}$$

where f_1 is the mole fraction of monomer 1 in the reaction medium. However, this transformation comes with a huge limitation associated with the experimental noise, affecting the precision of the estimates.[38]

1.3.4.2 Original and Extended Kelen-Tüdös Method

This method proposes a visual determination of the copolymerization constants when fitting the experimental data with the composition equation. It also overcomes the shortcoming of the FM method that arises from the unequal weighting of the experimental data.[39]

Despite its nice visualization, the original KT method can only be used as initial guesses at low conversion copolymerizations. Later on, Kelen and Tüdös extended their original equation to a new form that could handle higher conversions by introducing a conversion-dependent variable that calculates the partial molar conversions of the individual monomers.[40]

Regardless of their simplicity, all the methods derived from the linearization of the instantaneous copolymer composition equation are not statistically valid because the independent variable will always have error and the dependent variable could not have a constant variance.

1.3.4.3 Nonlinear Least-Squares Methods

Over the years, these methods have gained more attention as reliable estimation techniques compared to the previous linearized equations. They, in general, apply three assumptions: 1) the model sufficiently defines the experimental data, 2) the errors associated with the dependent variable are normally distributed and statistically independent on each run, and 3) the dependent variable should always have a constant variance.[41] Behnken[36] was the first to propose a method using this concept. A year later, Tidwell and Mortimer developed a method that modified the curve-fitting approach with a unique computational procedure that gives the same values of r_1 and r_2 every time after minimizing the sum of squares of the differences between the experimental and computed polymer compositions.[38] This procedure starts with giving initial estimates of reactivity ratios that could be obtained by other methods, using them to run many iterations, and leading to the optimum values of r_1 and r_2. Another interesting extension to the NLLS approach is the method proposed by Van der Meer et al.[42] (VLG) through the use of the error-in-variables-model (EVM), which employs the integrated copolymer composition.

VLG's method was developed to consider all sources of error in both variables using a nested-iterative algorithm that minimizes the weighted sum of squares of the distance between the observed and estimated values. However, Patino-Leal et al.[43] pointed out a disadvantage related to VLG's approach of applying EVM regarding the presence of additional unknown parameters that requires more optimization routines to get the optimal estimates. To tackle this problem, they proposed a refined EVM method that solves for only r_1 and r_2 and eliminates all other unknown parameters. This approach was the cornerstone for developing a user-friendly program written in

Fortran by Dube et al. to estimate reliable values of reactivity ratios.[44] A few years later, Police et al.[33] updated the program with a new version that included many features for easier and more powerful computation. Kazemi et al.[45–47] took the program applicability to another level with the launch of a new updated version written on MATLAB platform that gives the user more programming freedom. To highlight the program's features and accessibility, Scott and Penlidis provided a detailed description of the program and its requirements, supported by an intensive analysis of five case studies.[35]

Other approaches have also been published in the literature; Habibi et al.[48] suggested that since the NLLS methods are computational iterative processes that consume plenty of time and require a suitable initial guess of reactivity ratios, a generalized least squares (GLS) approach could be used to attain the same purpose. The GLS approaches were also investigated by Ashenagar et al.[49] who compared the reactivity ratios of styrene and 2-ethylhexyl acrylate copolymers computed by ordinary and generalized least square approaches to the EVM method. They concluded that the GLS approaches show a better agreement of estimation with the EVM method. Uozumi and Soga proposed a unique approach to estimate the reactivity ratios of three polymer products, including ethylene/1-hexene copolymers from ^{13}C NMR spectra as:

$$r_E = \frac{2[EE]}{[EH]X} \tag{2.3}$$

$$r_H = \frac{2[HH]X}{[EH]} \tag{2.4}$$

where $[EE]$, $[EH]$, and $[HH]$ represent the diad sequence distributions in the copolymer, and X is the feed concentration ratio of ethylene to hexene.[50] The application of ^{13}C NMR spectroscopy in determining the reactivity ratios was also involved in another approach developed by Al-Saleh et al.[51] where it is used to measure the comonomer sequence length distribution (CSLD). The estimation process is built upon an integrated deconvolution estimation model that consists of two steps. In the first step, the number of site types and polymer fractions made on each of them are determined by deconvoluting the copolymer MWD into several Flory's most probable distributions. The model then deconvolutes the CSLD of the copolymer and estimates the reactivity ratio of each component per site type. Beckingham et al.[52,53] utilized the nonterminal

model of copolymerization kinetics to derive integrated expressions that estimate the monomer reactivity ratios through a full range of conversions.

Mehdiabadi et al.[54] proposed a dynamic mathematical model that estimates the reactivity ratios by solving a system of ordinary differential equations for ethylene/1-hexene copolymers made with a supported metallocene catalyst. Their methodology was adopted in this thesis to estimate the reactivity ratios for ethylene/1-hexene and ethylene/1-octene copolymers made with CGC catalyst.

Chapter 2: Polymer Synthesis and Characterization

2.1 Introduction

Copolymers of ethylene/1-hexene and ethylene/1-octene were synthesized using two catalytic systems, CGC/MMAO and CGC/B/TOA, in a stainless-steel autoclave reactor operated in semi-batch mode.

The polymer samples were characterized by gel permeation chromatography equipped with an infrared detector (GPC-IR) to determine their molecular weight distributions (MWDs) and short-chain branching distributions (SCBDs). Details of the polymer synthesis procedures and analysis are given below.

2.2 Polymer Synthesis

2.2.1 Materials

Modified methylaluminoxane (MMAO, 7 wt % in toluene), tryisobutylaluminum (TIBA), and trioctylaluminum (TOA) were purchased from Sigma-Aldrich and used as received. Dimetylanilinium tetrakis (pentafluorophenyl) borate was provided by ExxonMobil as a solid and dissolved in distilled toluene. Ethylene and nitrogen (Praxair) were purified by flowing through packed beds of molecular sieves (3, 4 Å) and copper (II) oxide. HPLC grade toluene (99.9% purity, Sigma-Aldrich) was purified by refluxing it over n-butyllithium/styrene/sodium system for at least 24 hours and then distilling it under a nitrogen atmosphere. 1-Hexene and 1-octene with a purity of 97% and 98%, respectively, were purchased from Sigma-Aldrich and stored in a sealed bottle half-filled with dried 4 Å molecular sieves to absorb any residual impurities. The catalyst, dimethylsilyl(N-tert-butylamido)(tetramethylcyclopentadienyl)titanium dichloride (CGC), was purchased from Boulder Scientific as a powder and dissolved in purified toluene to the polymerization concentration. All air-sensitive materials were kept and handled in a glove box under an inert atmosphere.

2.2.2 Polymerization Procedure

All copolymers were made in a 300 mL Parr autoclave reactor equipped with an electrical band heater and internal cooling coil to keep the temperature under control (Figure 3.1). The reactor also has a pitched-blade impeller connected to a magneto-driver stirred, rotating at 700 rpm to maintain the mixing of the reaction medium. Before each polymerization, the reactor was pressurized with nitrogen and evacuated seven times to reduce the concentration of polar impurities inside it. Next, the reactor was washed by filling it with 150 mL of toluene and 0.5 g of TIBA that works as a scavenger, heating up to 140 °C and kept constant for 15 minutes. This ensures the removal of any left impurities at the reactor walls. Finally, the reactor contents were blown out under nitrogen pressure and the temperature was lowered to 60 °C through pressurizing and evacuating with nitrogen.

In a typical polymerization run of the CGC/MMAO catalytic system, toluene, MMAO, and comonomer (1-hexene or 1-octene) were injected into the reactor by differential pressure using a double-tipped transfer needle. Appropriate amounts of MMAO and the comonomer were prepared inside the glove box and placed in separate 20 mL glass vials sealed with rubber stoppers and crimp caps before their transfer to the reactor. The catalyst was transferred to the catalyst injection cylinder and kept there until the reactor contents were saturated with ethylene. For that to happen, the polymerization temperature was set to 120 °C, and the reactor contents of solvent, cocatalyst, and the comonomer started to mix. Once the temperature setpoint was reached, it was left to stabilize for two minutes before feeding the reactor with ethylene. To start the polymerization, the ethylene feed valve was closed and the catalyst injection cylinder valve was immediately opened to allow the catalyst to drop into the reactor through a pressure differential. This process should take a few seconds to reopen the ethylene feed valve and start making polymers. At the beginning of the polymerization, a 1-2 °C temperature increase was recorded due to the exothermic reactions associated with this process. However, this disturbance was promptly resolved by a control loop in the LabView program that keeps the temperature at 120 ± 0.1 °C throughout the polymerization. At the end of the polymerization, the reaction was stopped by closing the ethylene feed valve, stopping the reactor stirrer, and immediately blowing out the reactor contents into a 1 L beaker filled with 200 mL of ethanol to precipitate the polymer. The polymer suspension was then filtered and dried overnight inside the fume hood and finally in an oven of 70 °C under vacuum.

For CGC/B/TOA catalytic system, the only difference from the former system is the technique of adding the catalyst and cocatalyst to the reactor mixture. In this system, a simultaneous addition was applied where catalyst and borate solutions were mixed in one vial and injected into the catalyst injection cylinder. Moreover, TOA (scavenger) was added to the same vial of the comonomer and transferred together into the reactor. The rest procedures were the same as for the CGC/MMAO system.

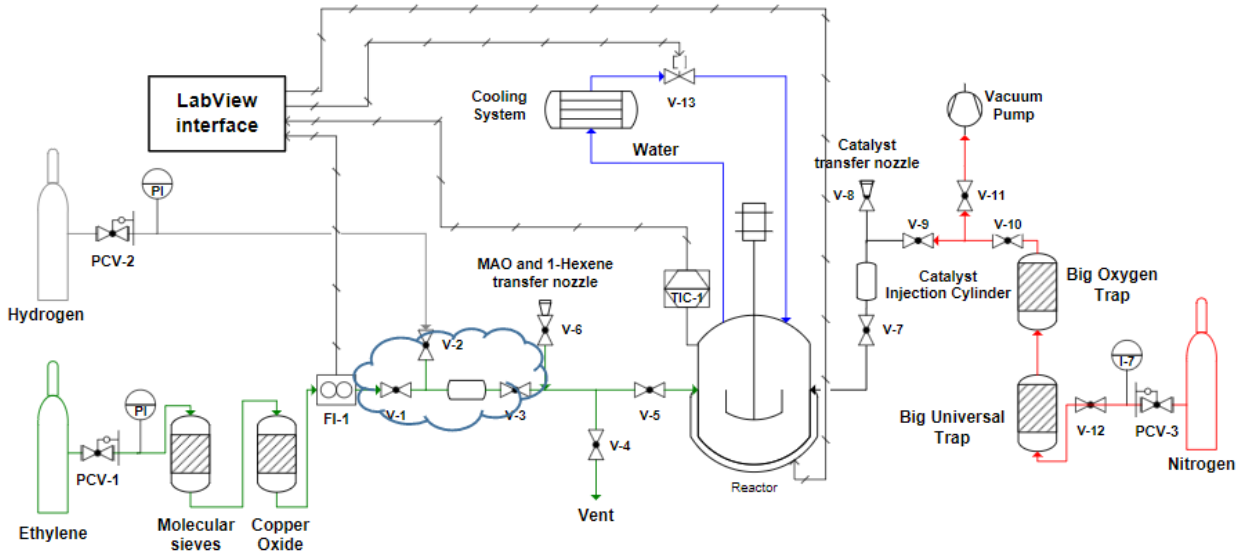

Figure 2.1 Schematic diagram of the reactor.[62]

2.3 Polymer Characterization

Molecular weight distribution (MWD) and short-chain branching distribution (SCBD) are two of the main microstructural properties that describe any polyolefin. A brief overview of the techniques used to measure these properties is given below.

2.3.1 Molecular Weight Distribution

The MWD is the most fundamental microstructural distribution of polyolefins due to the high impact it has on their mechanical and rheological properties. It is commonly determined with high-temperature size exclusion chromatography (SEC), also known as high-temperature gel permeation chromatography (GPC) (Figure 3.2). GPC is an analytical technique that separates the polymer chains according to their hydrodynamic volumes in solution.[55,56] For a typical analysis, a GPC unit from Polymer Char, equipped with three linear columns (Agilent PLgel Olexis, 7.5×300 mm, 13 µm particles) and three detectors (infrared, light scattering, and differential viscometer), was used. PE samples were prepared in 10 mL vials as dilute solutions using distilled trichlorobenzene (TCB) as solvent. The dilute solutions were then injected into a continually flowing stream of TCB (mobile phase) at a flow rate of 1 mL/min and an oven temperature of 145 °C. The solutions pass through a series of columns packed with millions of highly porous gel particles (stationary phase). As the flow continues, separation takes place with the large size particles eluting first from the columns while the small molecules penetrate into more pores and take longer elution time. This time depends on the volume of polymer coils in the solution. Hence, calibration curves of narrow MWD polystyrene standards and the universal calibration curve were used to relate the molecular weight to elution volume.[57]

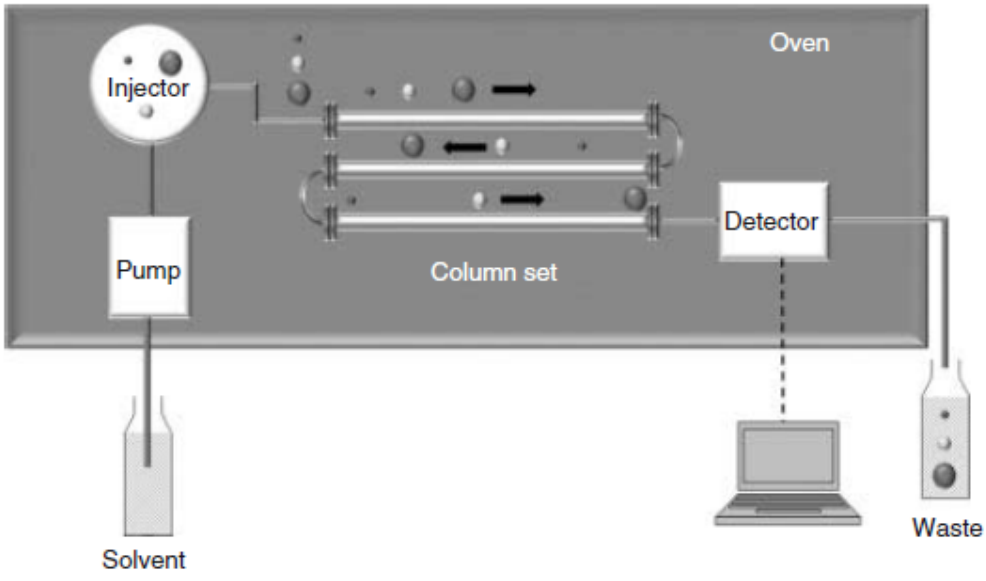

Figure 2.2 High-temperature gel permeation chromatography schematic.[2]

2.3.2 Short-Chain Branching Distribution

The short-chain branching in LLDPE is attributed to the α-olefins incorporation on the backbone of PE chains, influencing its morphology and physical properties such as density, melting point, hardness, permeability, and environmental stress cracking resistance.[58,59] The distribution of these chains was determined as a function of molecular weight using an IR detector coupled with the GPC unit. The technique relies on the absorption bands of methyl and methylene groups found between the 3000 and 2800 cm^{-1} spectral region, known as the C-H stretching region using TCB as the mobile phase.[60,61] A calibration curve was used to determine the SCBD of the copolymer samples. The curve was built using ethylene/1-hexene and ethylene/1-octene copolymer samples of known SCB frequency made with CGC catalyst. For the reference point of zero SCB frequency, three ethylene homopolymers and two linear polyethylene standards were produced with the same catalyst. ^{13}C NMR was used to measure the SCBD of these calibration standards. The SCB frequency in the polymer, which is expressed as the number of SCB per 1000 C atoms in the chain, was used to calculate the comonomer molar fraction (F_2) using Eq. (2.1),

$$F_2 = \frac{2 \times SCB}{1000 + (2 - n_c) \times SCB} \tag{2.1}$$

where n_c is the number of carbons in the comonomer (n_c = 6 for 1-hexene and 8 for 1-octene).

Chapter 3: A Dynamic Model to Estimate the Reactivity Ratios of Ethylene/1-Hexene Copolymers

3.1 Introduction

Two catalytic systems and six sets of copolymerizations were used to estimate the reactivity ratios of ethylene/1-hexene at high composition drift using a dynamic mathematical model. An extra set, for the case of low composition drift, was also used to find out how the dynamic model estimates the reactivity ratios compared to the traditional Mayo-Lewis equation approach at low conversions. All polymerization runs were performed using the same catalyst, CGC, but two different cocatalysts, MMAO or borate.

3.2 Copolymerization with CGC/MMAO

The first two sets of copolymers were made with MMAO as the cocatalyst, varying the 1-hexene content on one set and the polymerization time on the other. Later both sets were combined to form a third set introduced to the model.

3.2.1 Effect of 1-Hexene Concentration

Seven copolymers with different 1-hexene concentrations were made under a fixed polymerization time of 15 minutes to investigate the effect of varying 1-hexene concentrations on polymer yield, molecular weight, and ultimately determine their reactivity ratios. Table 3.1 summarizes the polymerization conditions of this set. The ID of each run consists of two parts: the first refers to the polymerization replicate (2 means the second replicate), whereas the second represents 1-hexene reactor loading, from 0 to 10 g.

Table 3.1 Polymerization conditions for ethylene/1-hexene copolymers made with CGC/MMAO at different 1-hexene concentrations.

Run	1-Hexene (g)	Catalyst (g)	Yield (g)
R1-H4	3.978	0.404	7.61
R1-H8	7.891	0.403	10.76
R1-H10	9.883	0.406	8.91
R2-H4	4.016	0.402	8.83
R2-H2	1.991	0.408	6.88
R1-H2	1.970	0.404	6.78
R1-H0	0.000	0.406	4.49

T = 120 °C, P_E = *120 psig, [MMAO]/[CAT] = 7252.94, t = 15 min.*

The 1-hexene loading in Table 3.1 represents the amount of 1-hexene fed into the reactor at the beginning of the polymerizations. Figure 3.1 shows that the mass of 1-hexene added to the reactor and the concentration of 1-hexene in toluene follow a linear relationship, as estimated using the Peng-Robinson equation of state available in Aspen Hysys.

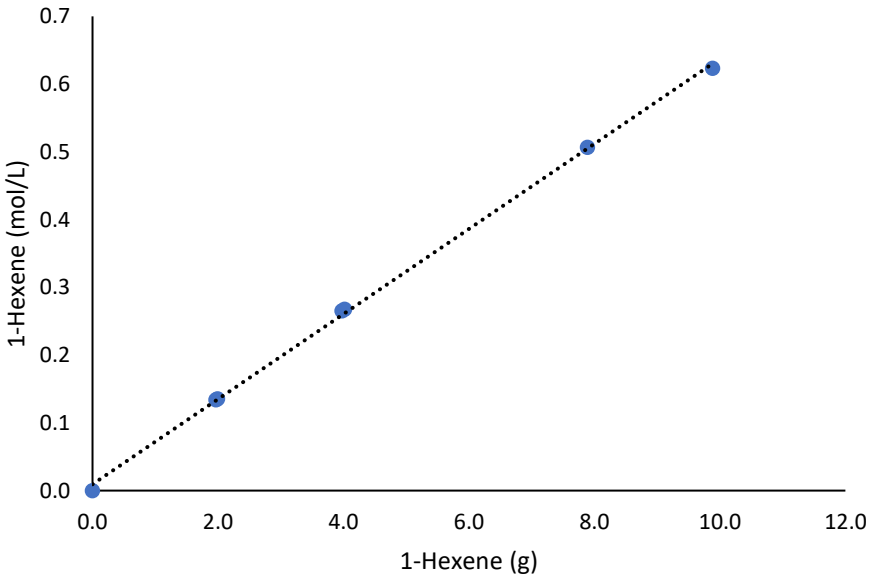

Figure 3.1 Concentration of 1-hexene in toluene versus the amount of 1-hexene fed to the reactor at 120 °C for CGC/MMAO.

Polymer yield increases proportionally with 1-hexene concentration in toluene, as shown in Figure 3.2. This relationship seems to start to break down at higher concentrations of 1-hexene (run R1-H10), likely because the amount of poisons and impurities increase when more 1-hexene fed to the reactor. Even if no poisons were introduced with 1-hexene, the yield would eventually start to decrease as 1-hexene is less reactive than ethylene.

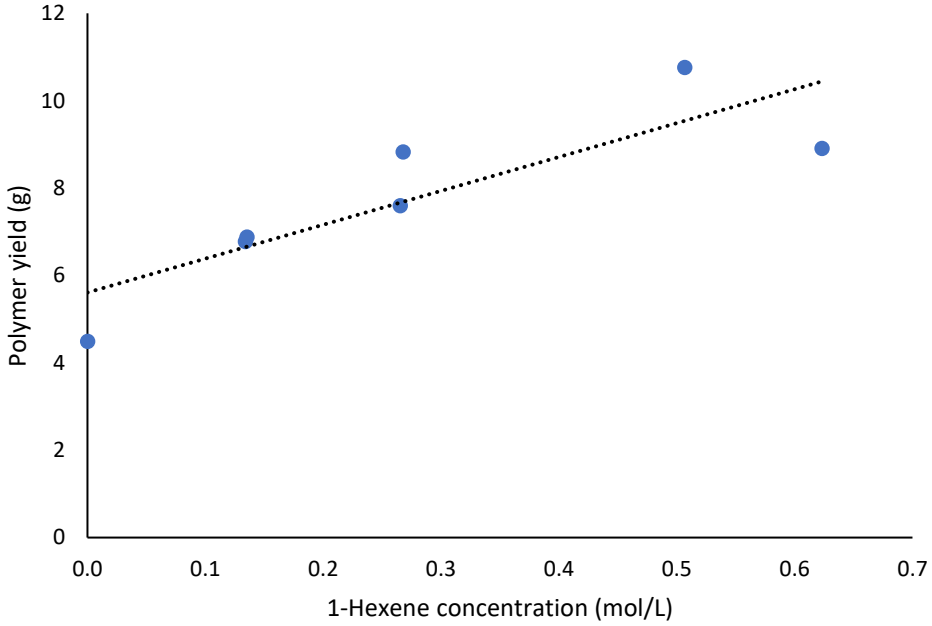

Figure 3.2 Polymer yield as a function of 1-hexene concentration for CGC/MMAO.

The GPC unit equipped with the IR detector provided the molecular weight data for the samples listed in Table 3.1. The weight (M_w) and number (M_n) average molecular weights decrease with increasing 1-hexene concentration in the polymerization medium, indicating that transfer to 1-hexene plays an important role in this system (Table 3.2 and Figure 3.3).

Table 3.2 Molecular weight averages and SCB frequencies for CGC/MMAO system at different 1-hexene concentrations.

Run	M_w	M_n	PDI	SCB/1000C
R1-H4	98601	43405	2.27	28.6
R1-H8	69691	31289	2.23	47.3
R1-H10	60573	28566	2.12	60.2
R2-H4	88252	36290	2.43	24.8
R2-H2	123017	46584	2.64	14.3
R1-H2	132177	54161	2.44	15.3
R1-H0	217564	87785	2.48	0.00

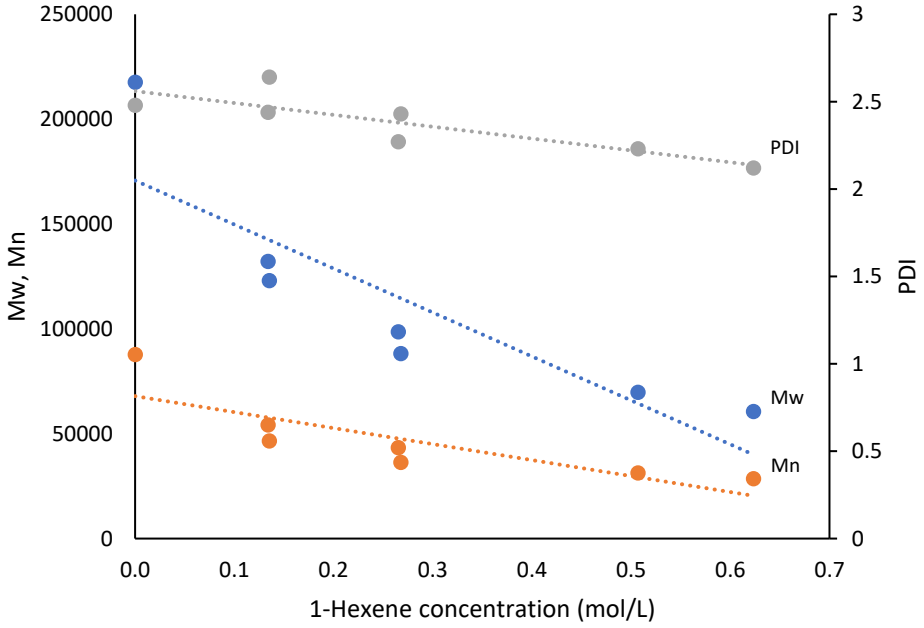

Figure 3.3 M_w, M_n, and PDI versus 1-hexene concentration for CGC/MMAO system.

The MWD and SCBD of these samples were also obtained using GPC-IR. Figure 3.4 displays the wide range of SCB frequencies and distributions for different 1-hexene loadings. It also shows that narrow MWD of these samples confirm that the catalyst has only one type of active site.

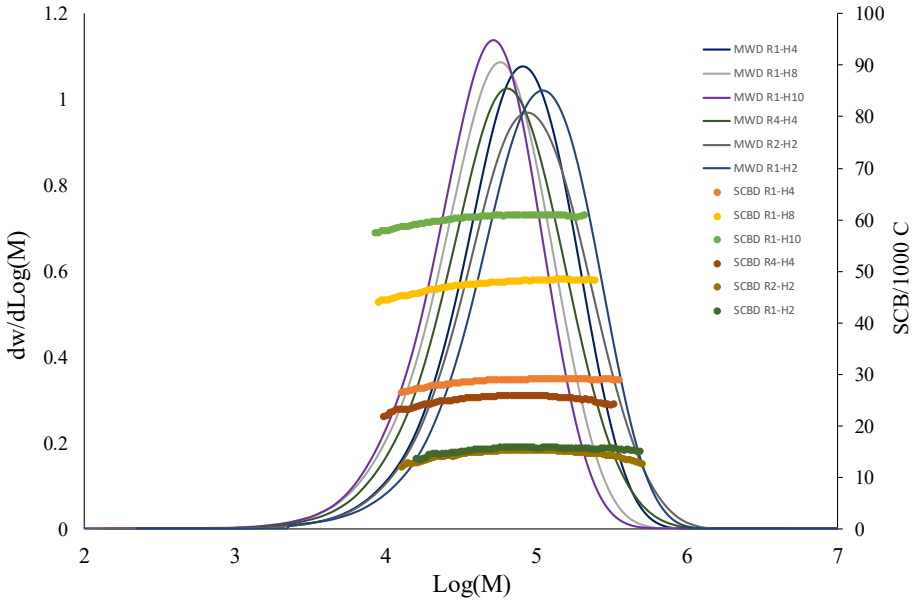

Figure 3.4 MWD and SCBD for the samples listed in Table 3.1.

3.2.1.1 Estimation of Reactivity Ratios

To estimate the reactivity ratios, we first calculated the molar fraction of 1-hexene in the liquid phase at the beginning of polymerization, $f_{2\circ}$, using Eq. (3.1).

$$f_{2\circ} = \frac{[M_2]}{[M_1] + [M_2]} \tag{3.1}$$

where $[M_1]$ and $[M_2]$ are the concentrations of ethylene and 1-hexene in toluene, respectively. The values of $f_{2\circ}$ for each run are tabulated in the sixth column of Table 4.3. The fifth column lists the mole fraction of 1-hexene in the copolymer, F_2, based on the SCB/1000 C obtained by GPC-IR and calculated using Eq. (2.1) described in Chapter 2. The final 1-hexene mass (unreacted 1-hexene) at the end of polymerization was calculated by subtracting the 1-hexene mass incorporated in the polymer product from the initial 1-hexene mass fed to the reactor at equilibrium. The final f_2 values were computed using the concentrations of ethylene and 1-hexene in the liquid phase at the end of polymerization. These concentrations were estimated by a trial-and-error in Aspen Hysys, given that the system consists of four non-polymeric components (ethylene, 1-hexene,

toluene, and nitrogen) and that the polymerization temperature and pressure, reactor volume, and final 1-hexene mass were known.

Table 3.3 Mass and molar balances for 1-hexene consumption at the beginning and end of polymerization for CGC/MMAO system at different 1-hexene concentrations.

Run	Initial 1-Hexene (g)	Final 1-Hexene (g)	% Change in 1-Hexene mass	F_2	f_{2o} Initial	f_2 Final
R1-H4	3.978	2.674	32.79	0.065	0.479	0.379
R1-H8	7.891	4.831	38.73	0.117	0.644	0.524
R1-H10	9.883	6.664	32.57	0.159	0.693	0.602
R2-H4	4.016	2.701	32.74	0.055	0.482	0.382
R2-H2	1.991	1.401	29.63	0.030	0.316	0.243
R1-H2	1.970	1.347	31.61	0.033	0.314	0.236
R1-H0	0.000	0.000	0.00	0.000	0.000	0.000

The material balance for 1-hexene in the liquid phase inside the reactor is,

$$\frac{-F_2}{1-F_2}\frac{PQ}{RT} = \frac{\mathrm{d}(V_R[M_2])}{\mathrm{d}t} \tag{3.2}$$

The term, $\frac{PQ}{RT}$, in Eq. (3.2) represents the rate of polymerization (mol/s) using the ideal gas law to convert the volumetric flow rate (L/s) to molar flow rate (mol/s), where P is the atmospheric pressure (atm), Q is the flow rate of ethylene to the reactor (L/s), R is the universal gas constant (L.atm/K.mol), T is the room temperature (K), and V_R is the volume of the liquid phase in the reactor (L), which can be written as,

$$V_R = V_{R\circ}\,(1+\varepsilon t) \tag{3.3}$$

where $V_{R\circ}$ is the initial volume of the liquid phase and ε is a parameter that accounts for the change in reactor volume due to polymer formation with time. It can be computed via the following equation,

$$\varepsilon = \frac{Y_P}{t_P\,\rho_P V_{R\circ}} \tag{3.4}$$

where Y_P is the polymer yield (g), t_P is the total polymerization time (s), and ρ_P is the polymer density (g/cm^3).

The ethylene flow rate (Q) was fitted using the rational function in Eq. (3.5) via MatLab Curve Fitting Toolbox. A summary of these parameters and goodness of fit is provided in Appendix A.

$$Q = \frac{p_1 t^2 + p_2 t + p_3}{t^2 + q_1 t + q_2} \tag{3.5}$$

Substituting Eq. (3.3) and (3.5) in Eq. (3.2),

$$\frac{-F_2}{1 - F_2} \frac{P \dfrac{p_1 t^2 + p_2 t + p_3}{t^2 + q_1 t + q_2}}{R\,T} = \frac{d\big(V_{R\circ}\,(1 + \varepsilon t)[M_2]\big)}{\mathrm{d}t} \tag{3.6}$$

After some simplification steps, Eq. (3.6) becomes,

$$\frac{-F_2}{(1 - F_{2)}} \frac{P \dfrac{p_1 t^2 + p_2 t + p_3}{t^2 + q_1 t + q_2}}{R\,T} = V_{R\circ}\left[\varepsilon[M_2] + (1 + \varepsilon t)\frac{\mathrm{d}[M_2]}{\mathrm{d}t}\right] \tag{3.7}$$

Equation (3.1) can be used with the final molar fraction of 1-hexene, f_2, and rearranged to

$$[M_2] = [M_1]\frac{f_2}{1 - f_2} \tag{3.8}$$

The ethylene concentration in Eq. (3.8), $[M_1]$, is assumed to be constant as the ethylene pressure is kept constant during the polymerization. Taking the derivatives of both sides of Eq. (3.8) results in,

$$\frac{\mathrm{d}[M_2]}{\mathrm{d}t} = \frac{[M_1]}{(1 - f_2)^2}\frac{\mathrm{d}f_2}{\mathrm{d}t} \tag{3.9}$$

Substituting Eq. (3.9) in Eq. (3.7) gives,

$$\frac{-F_2}{1-F_2}\frac{P\dfrac{p_1t^2+p_2t+p_3}{t^2+q_1t+q_2}}{R\,T}=V_{R\circ}\left[\varepsilon[M_2]+(1+\varepsilon t)\frac{[M_1]}{(1-f_2)^2}\frac{\mathrm{d}f_2}{\mathrm{d}t}\right] \tag{3.10}$$

Equation (3.10) can be rearranged to,

$$\frac{-F_2}{1-F_2}\frac{P\dfrac{p_1t^2+p_2t+p_3}{t^2+q_1t+q_2}}{R\,T}-V_{R\circ}\varepsilon[M_2]=V_{R\circ}(1+\varepsilon t)\frac{[M_1]}{(1-f_2)^2}\frac{\mathrm{d}f_2}{\mathrm{d}t} \tag{3.11}$$

which can also be written as,

$$\frac{\mathrm{d}f_2}{\mathrm{d}t}=\left(\frac{-F_2}{1-F_2}\frac{P\dfrac{p_1t^2+p_2t+p_3}{t^2+q_1t+q_2}}{R\,T}-V_{R\circ}\varepsilon[M_2]\right)\frac{(1-f_2)^2}{V_{R\circ}(1+\varepsilon t)[M_1]} \tag{3.12}$$

Recalling Eq. (3.8) for $[M_2]$, Eq, (3.12) can be simplified to,

$$\frac{\mathrm{d}f_2}{\mathrm{d}t}=-\frac{(1-f_2)^2}{1+\varepsilon t}\left\{\frac{F_2}{1-F_2}\frac{P\dfrac{p_1t^2+p_2t+p_3}{t^2+q_1t+q_2}}{R\,T\,V_{R\circ}\,[M_1]}+\frac{\varepsilon f_2}{1-f_2}\right\} \tag{3.13}$$

The instantaneous mole fraction of 1-hexene in the polymer, F_2, can be substituted with the instantaneous mole fraction in the liquid phase, f_2, via Eq. (3.14),

$$F_2=\frac{\mathrm{r}_2f_2^2+(1-f_2)f_2}{\mathrm{r}_2f_2^2+2\,(1-f_2)f_2+r_1(1-f_2)^2} \tag{3.14}$$

Substituting Eq. (3.14) in Eq. (3.13) leads to the final equation used to estimate the reactivity ratios, r_1 and r_2, under substantial composition drift,

$$\frac{\mathrm{d}f_2}{\mathrm{d}t}=-\frac{(1-f_2)^2}{1+\varepsilon t}\left\{\frac{\dfrac{r_2f_2^2+(1-f_2)f_2}{r_2f_2^2+2(1-f_2)f_2+r_1(1-f_2)^2}}{1-\dfrac{r_2f_2^2+(1-f_2)f_2}{r_2f_2^2+2\,(1-f_2)f_2+r_1(1-f_2)^2}}\frac{P\dfrac{p_1t^2+p_2t+p_3}{t^2+q_1t+q_2}}{R\,T\,V_{R_0}\,[M_1]}+\frac{\varepsilon f_2}{1-f_2}\right\} \tag{3.15}$$

A system of six ordinary differential equations was generated by solving Eq. (3.15) for the polymerization runs listed in Table 3.1 with 4th order Runge-Kutta method. The solutions were based on minimizing the sum of squares of residuals between the final experimental values of f_2 and the model predictions, while changing the value of parameters r_1 and r_2. The estimated values of r_1 and r_2 were 23.817 and 0.160, respectively, and the sum of squared errors for the estimation was 6.50×10^{-5}.

Figure 3.5 shows how f_2 changes for different initial values during the polymerization using the estimated reactivity ratios. The black dots at the end of each run are the experimental values measured for f_2 as explained at the beginning of this section. Model predictions and experiments agree very well, as shown in Figure 3.6.

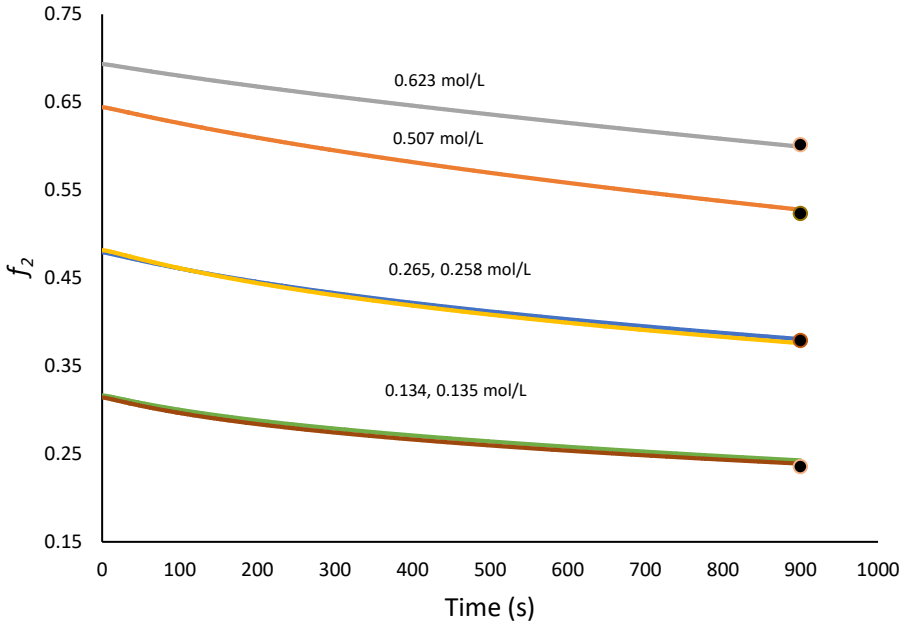

Figure 3.5 1-Hexene molar fractions for ethylene/1-hexene copolymerizations with CGC/MMAO as a function of time.

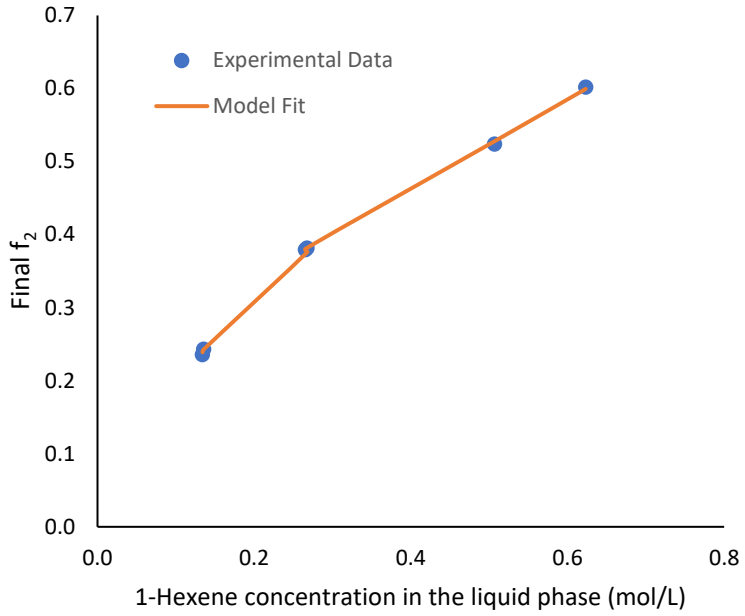

Figure 3.6 Comparison between experimental and model final f_2 values for copolymerizations with CGC/MMAO.

3.2.2 Effect of Polymerization Time

Four polymerizations using the same 1-hexene concentration were ran for different times to investigate the effect of time on polymer microstructure and to estimate reactivity ratios. The initial 1-hexene concentration was 0.3879 mol/L in all runs, whereas the polymerization time was increased in 3 minutes increments, from 3 to 12 minutes, as listed in Table 3.4. Catalyst and cocatalyst concentrations, temperature, and ethylene pressure were the same for all runs.

Table 3.4 Polymerization conditions for ethylene/1-hexene copolymers made with CGC/MMAO at different polymerization times.

Run	Duration (min)	Catalyst (g)	Yield (g)
R1-H6	3	0.401	4.3
R2-H6	6	0.402	6.62
R3-H6	9	0.405	8.02
R4-H6	12	0.403	9.86

T = 120 °C, P_E = 120 psig, [MMAO]/[CAT] = 7252.94, 1-hexene = 0.3879 mol/L.

Figure 3.7 shows that the polymer yield increases with polymerization time, as expected.

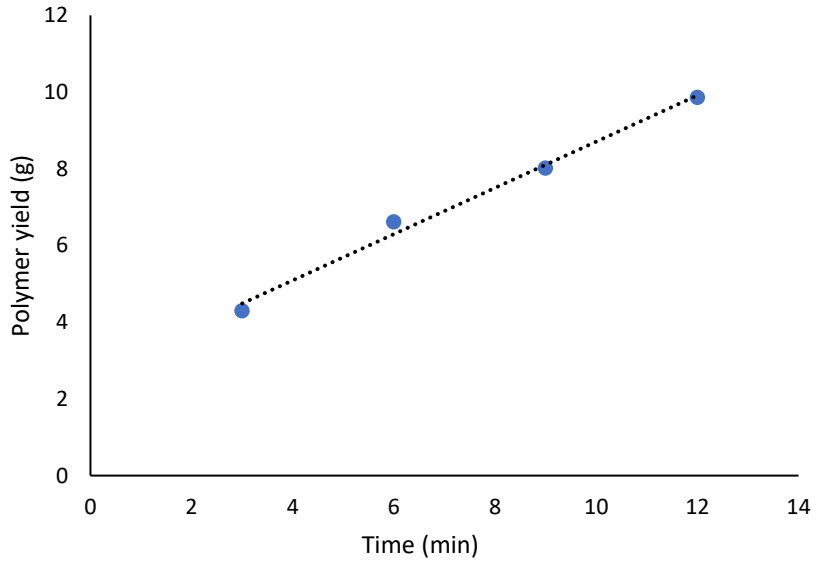

Figure 3.7 Polymer yield versus polymerization time for CGC/MMAO.

The copolymers were characterized by GPC to measure their molecular weight averages and SCBs. These results are summarized in Table 4.5 and Figure 3.8.

Table 3.5 Molecular weight averages and SCB frequencies for ethylene/1-hexene copolymers made with CGC/MMAO at different

Run	M_w	M_n	PDI	SCB/1000C
R1-H6	71423	31331	2.28	34.3
R2-H6	86353	37646	2.29	32
R3-H6	95193	42993	2.21	31.9
R4-H6	97510	44596	2.19	29.8

The molecular weight averages increased with polymerization time, since the concentration of 1-hexene in the reactor decreases with time and transfer to 1-hexene is important in this system, as already seen in Figure 3.3.

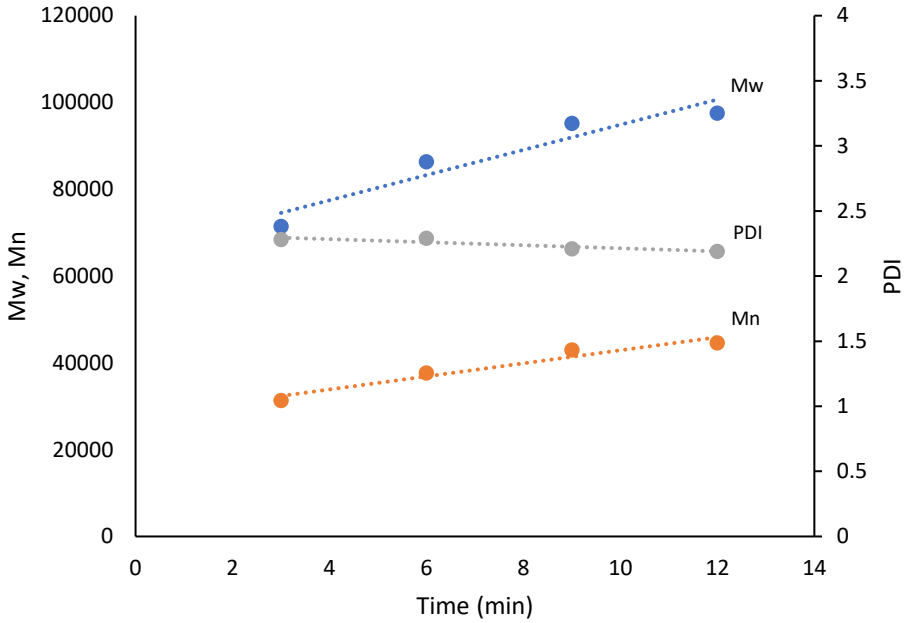

Figure 3.8 Molecular weight averages as a function of polymerization time for CGC/MMAO.

Likewise, the SCB frequencies decreased for longer polymerizations (Figure 3.9), since the concentration of 1-hexene in the reactor decreases with time.

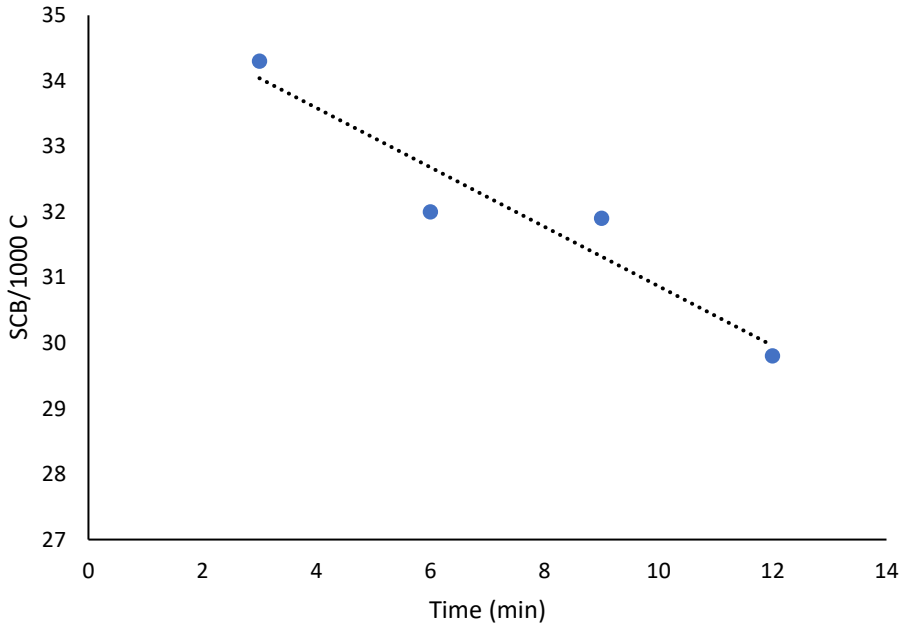

Figure 3.9 SCB frequency versus polymerization time for CGC/MMAO.

The GPC/IR plot in Figure 3.10 shows how the SCB frequency varies across the polymer MWD.

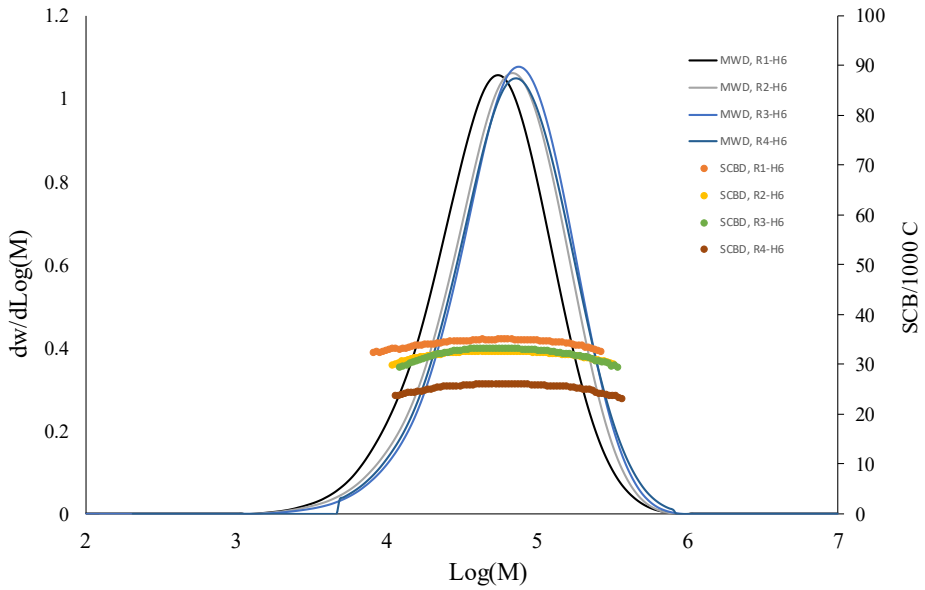

Figure 3.10 MWD and SCBD for the samples listed in Table 3.4.

3.2.2.1 Estimation of Reactivity Ratios

The same model derived in Section 3.2.1.1 was used to estimate the reactivity ratios for this set of copolymerizations. The SCB frequency (1-hexene incorporated in the copolymer) decreases with polymerization time, as illustrated from the fifth column of Table 3.6. The molar fraction of 1-hexene in the copolymer is also lower than in the previous set of copolymerization, with a maximum incorporation of 7.95 mol % and the range of f_2 values is significantly narrower, making it harder to estimate the reactivity ratios.

Table 3.6 Mass and molar balances for 1-hexene consumption at the beginning and end of polymerization for CGC/MMAO at different times.

Run	Initial 1-Hexene (g)	Final 1-Hexene (g)	% Change in 1-Hexene mass	F_2	f_{2o} Initial	f_2 Final
R1-H6	5.919	5.034	14.952	0.0795	0.5771	0.5337
R2-H6	5.934	4.663	21.420	0.0734	0.5780	0.5148
R3-H6	5.922	4.387	25.922	0.0731	0.5772	0.4997
R4-H6	5.929	4.168	29.711	0.0677	0.5774	0.4871

Eq. (3.15) was used to generate a system of four ordinary differential equations using new regression parameters (see Appendix A). The model predictions for reactivity ratios were $r_1 = 24.612$ and $r_2 = 0.167$, with a sum of squared errors equal to 1.21×10^{-4}, which is higher than for the previous set of copolymerizations. Figure 3.11 compares experimental and model values for f_2 as a function of time.

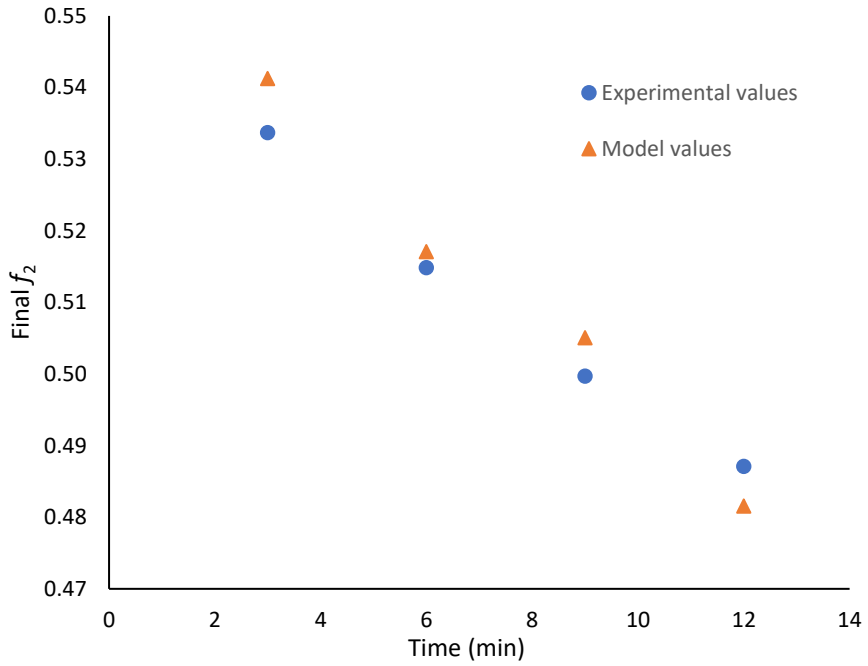

Figure 3.11 Comparison between experimental and model final f_2 values at different polymerization times for CGC/MMAO.

3.2.3 The combined set of polymerizations

To overcome the shortcomings of the second set of polymerizations, both sets were combined in one. The model was then used to generate a system of ten ordinary differential equations with a wider range of f_2 and F_2 values. The new and former estimates are compared in Table 3.7.

Table 3.7 Reactivity ratios estimates for ethylene/1-hexene copolymers made with CGC/MMAO.

	r_1	r_2	SSE
Set 1: Varying initial 1-hexene concentrations	23.817	0.160	6.50×10^{-5}
Set 2: Varying polymerization times	24.612	0.167	1.21×10^{-4}
Set 1+2	24.602	0.192	1.80×10^{-4}

The three approaches give close estimates, with the first set having the lowest SSE value. The Mayo-Lewis plot in Figure 3.12 confirms that the three sets provide almost identical predictions for the molar fraction of ethylene in the copolymer, F_1.

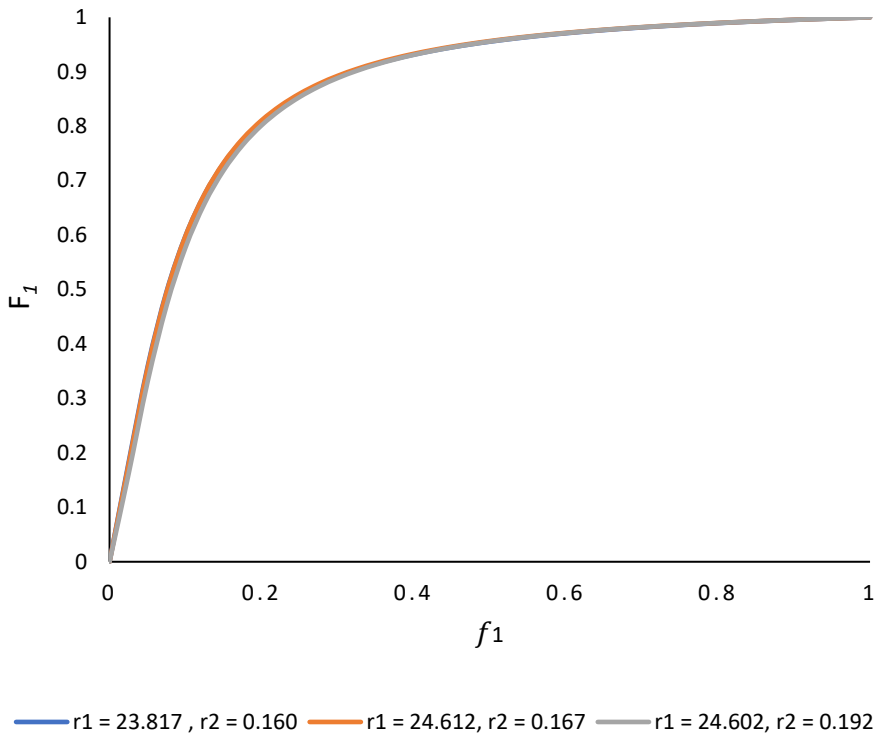

Figure 3.12 Ethylene molar fractions in the copolymer using the Mayo-Lewis equation for the three sets of reactivity ratios in Table 3.7.

3.3 Copolymerization with CGC/B/TOA

The other catalytic system investigated was CGC/B/TOA in the presence of trioctylaluminum (TOA) as a scavenger and alkylating agent. The first set of polymerizations was done under varying 1-hexene concentrations at the same polymerization time, and the second set under the same 1-hexene concentration and varying polymerization times.

3.3.1 Effect of 1-Hexene Concentration

Five copolymerizations were ran under four 1-hexene initial concentrations to investigate how they affected polymer yield and molecular weight, and to estimate reactivity ratios. The polymerization time of all runs was ten minutes. TOA was added to the reactor at the beginning of the polymerization. The polymerization conditions are shown in Table 3.8.

Table 3.8 Polymerization conditions for ethylene/1-hexene copolymers with CGC/borate at different 1-hexene concentrations.

Run	1-Hexene (g)	Catalyst (g)	Yield (g)
B1-H4	3.950	0.404	8.52
B1-H6	5.920	0.403	8.97
B1-H2	1.978	0.404	7.40
B1-H8	7.898	0.402	9.51
B2-H2	1.984	0.401	7.22

T = 120 °C, P_E = *120 psig, [Borate]/[CAT] = 8.64, TOA = 0.149 g, t = 10 min.*

The concentration of 1-hexene in the liquid phase increased linearly with the mass of 1-hexene fed into the reactor, as depicted in Figure 3.13.

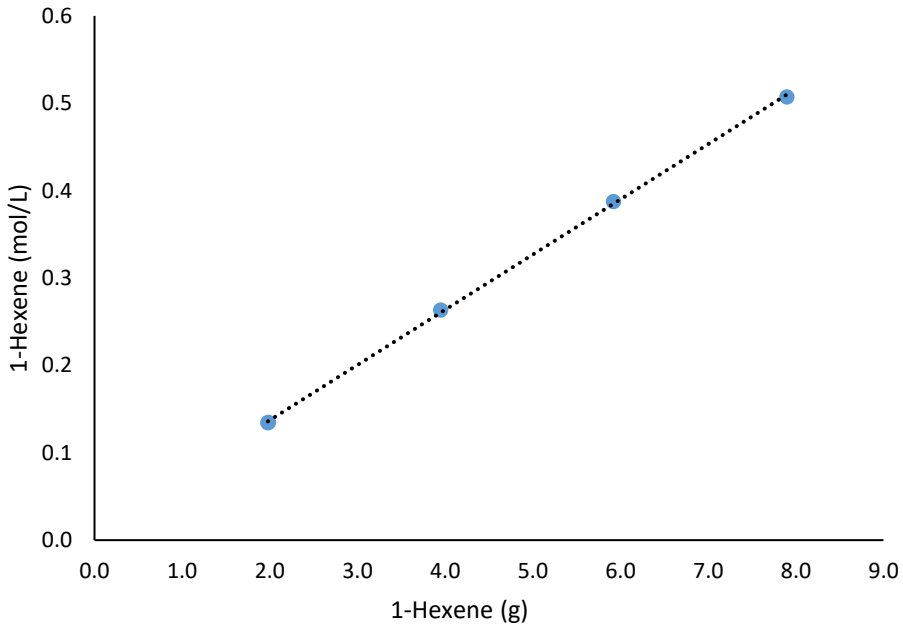

Figure 3.13 Concentration of 1-hexene in toluene versus mass of 1-hexene fed to the reactor at 120 °C.

Figure 3.14 show that the polymer yield increased proportionally to the concentration of 1-hexene in the reactor.

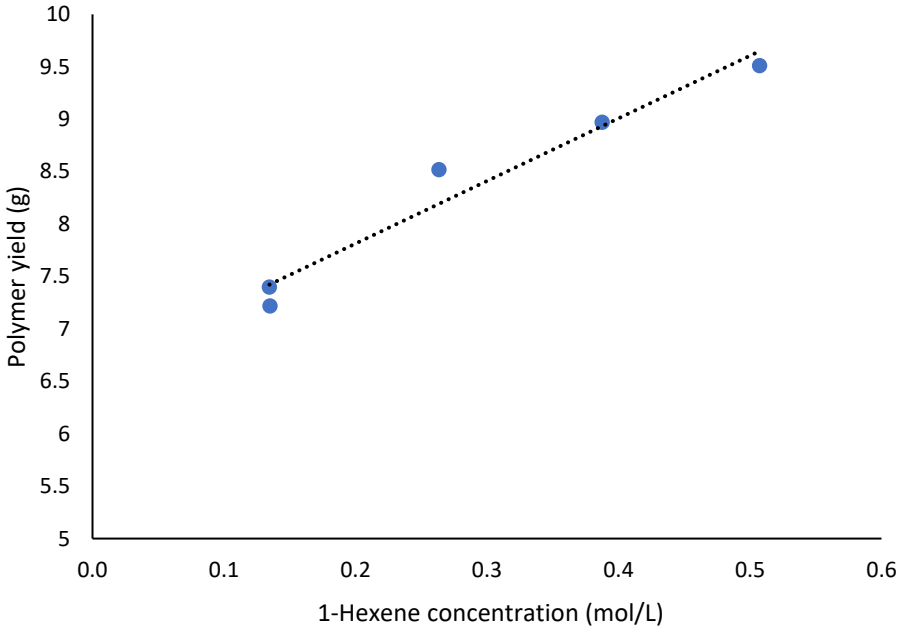

Figure 3.14 Polymer yield as a function of 1-hexene concentration for CGC/B/TOA.

According to the GPC-IR results in Table 3.9 and Figure 3.15, M_w and M_n decreased with increasing 1-hexene concentration in the polymerization medium.

Table 3.9 Molecular weight averages and SCB frequencies for ethylene/1-hexene copolymers made with CGC/borate system at different 1-hexene concentrations.

Run	M_w	M_n	PDI	SCB/1000C
B1-H4	95267	33644	2.83	9.5
B1-H6	89870	31970	2.81	13.7
B1-H2	137531	46836	2.94	5.1
B1-H8	78064	28328	2.76	17.3
B2-H2	120008	44722	2.68	5.1

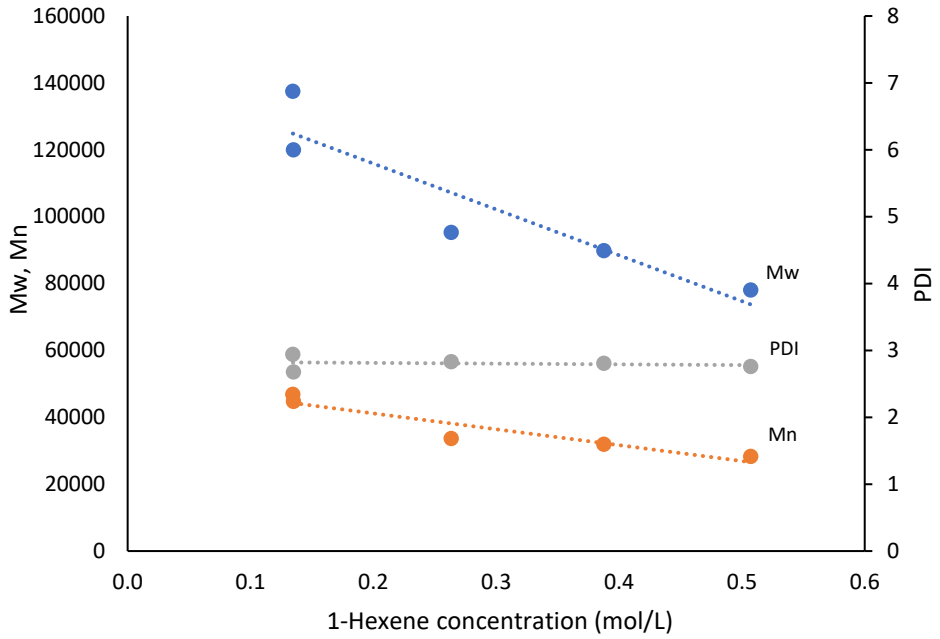

Figure 3.15 M_w, M_n, and PDI versus 1-hexene concentration for ethylene/1-hexene copolymers made with CGC/B/TOA.

The SCB frequency in the copolymers increase with 1-hexene concentration in the reactor, as shown in Figure 3.16.

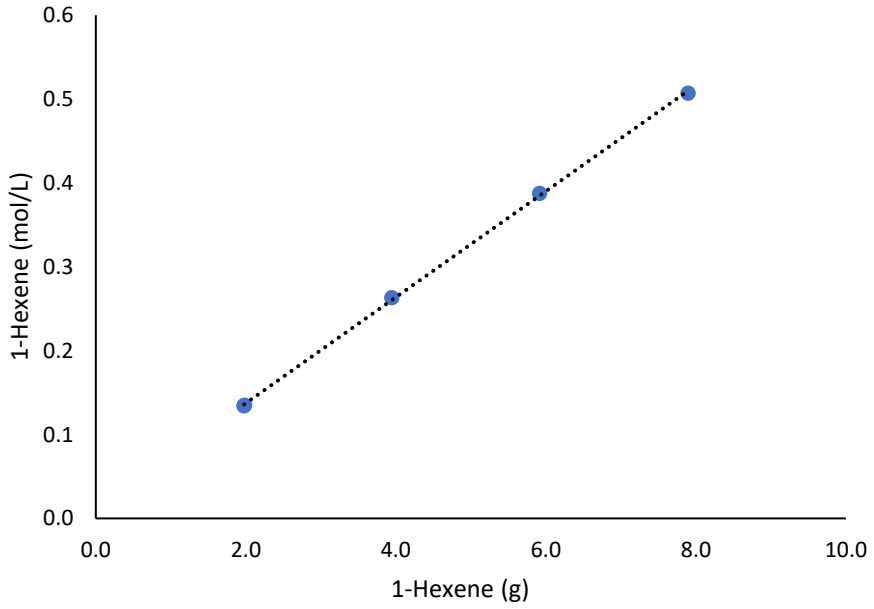

Figure 3.16 SCB frequency as a function of 1-hexene concentration in the reactor for ethylene/1-hexene copolymers made with CGC/B/TOA.

The SCB distribution along the MWD for these copolymers is depicted in Figure 3.17. The MWDs become slightly narrower when the concentration of 1-hexene increases, while the SCB frequency gradually increases.

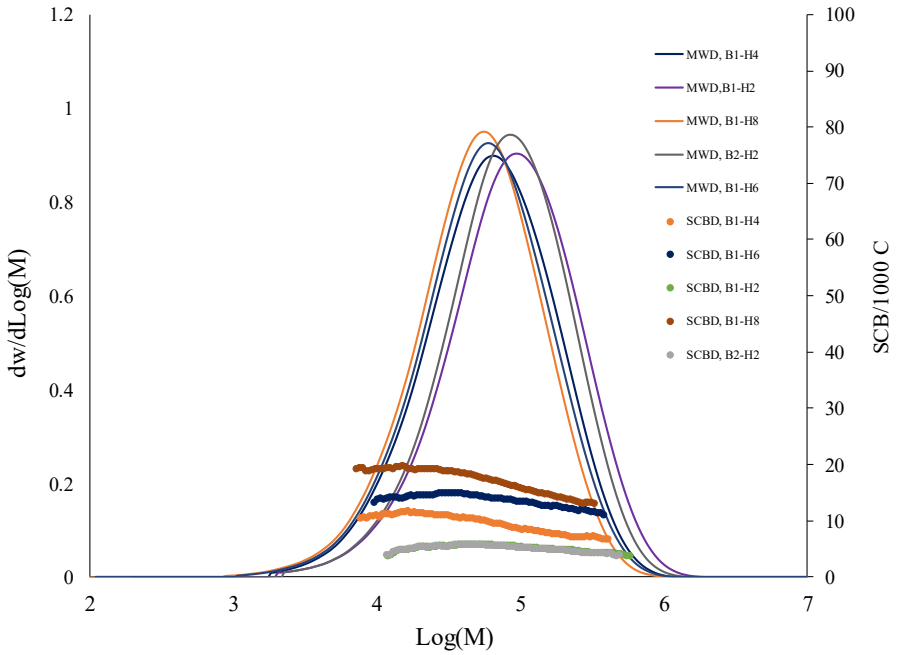

Figure 3.17 MWD and SCBD for the samples listed in Table 3.8.

3.3.1.1 Estimation of Reactivity Ratios

Table 3.10 shows that the composition drift with CGC/B/TOA is less pronounced than with CGC/MMAO. This is expected, since MMAO activates and stabilizes the metallocene sites more effectively than the borate. The 1-hexene molar fractions in the copolymers, F_2, are significantly lower than for CGC/MMAO, showing that CGC/B/TOA is not a good incorporator of 1-hexene.

Table 3.10 Mass and molar balances for 1-hexene consumption at the beginning and end of polymerizations with CGC/borate at different 1-hexene concentrations.

Run	Initial 1-Hexene (g)	Final 1-Hexene (g)	% Change in 1-Hexene mass	F_2	f_{2o} Initial	f_2 Final
B1-H4	3.950	3.464	12.297	0.0198	0.478	0.441
B1-H6	5.920	5.183	12.460	0.0290	0.577	0.541
B1-H2	1.978	1.751	11.438	0.0104	0.315	0.286
B1-H8	7.898	6.910	12.509	0.0372	0.645	0.610
B2-H2	1.984	1.764	11.122	0.0104	0.316	0.289

Figure 3.18 shows that Eq. (3.15) could predict the 1-hexene concentration drift well for this system, leading to the following estimates for reactivity ratios: $r_1 = 82.63$, $r_2 = 0.017$, and $SSE = 6.58 \times 10^{-6}$. The small SSE value can be visualized in Figure 3.19, comparing experimental and model values for the final f_2.

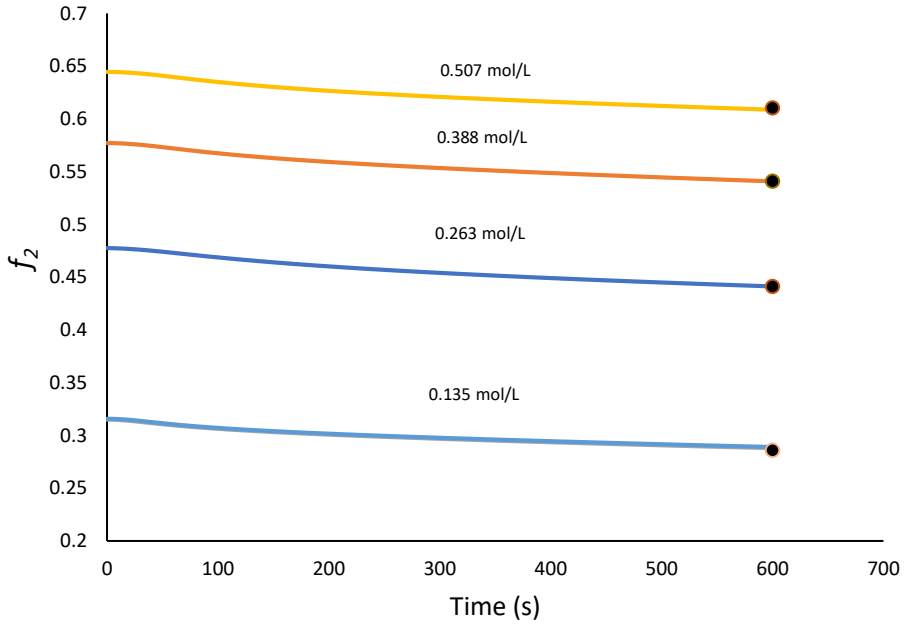

Figure 3.18 1-Hexene composition drift for polymerizations with CGC/B/TOA.

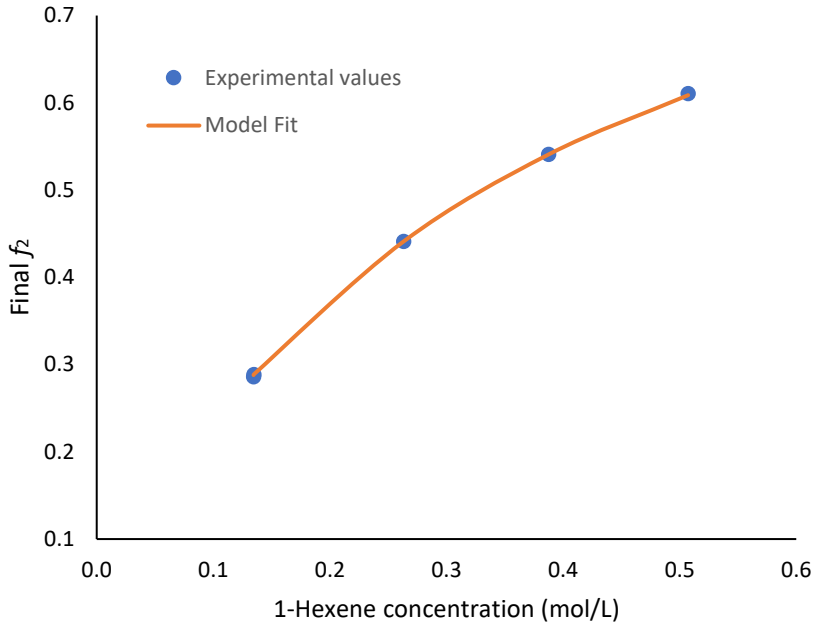

Figure 3.19 Comparison between experimental and model final f_2 values at different initial 1-hexene concentrations for copolymerization with CGC/B/TOA.

3.3.2 Effect of Polymerization Time

To investigate the effect of varying the polymerization time on the polymer yield, M_w and M_n, SCB, and reactivity ratios, four polymerizations at four different times were performed. Polymerization times were changed from 4 to 10 minutes by 2-minute increments randomly. Temperature, ethylene pressure, TOA, and cocatalyst/catalyst ratio were kept constant, as shown in Table 3.11.

Table 3.11 Polymerization conditions for ethylene/1-hexene copolymers made with CGC/B/TOA at different polymerization times.

Run	Duration (min)	Catalyst (g)	Yield (g)
B2-H4	6	0.402	7.42
B1-H4	10	0.404	8.52
B4-H4	8	0.403	7.97
B3-H4	4	0.403	6.46

T = 120 °C, P_E = 120 psig, [Borate]/[CAT] = 8.64, TOA = 0.149, 1-hexene = 0.2639 mol/L.

Figure 3.20 shows that polymer yield increases with polymerization time.

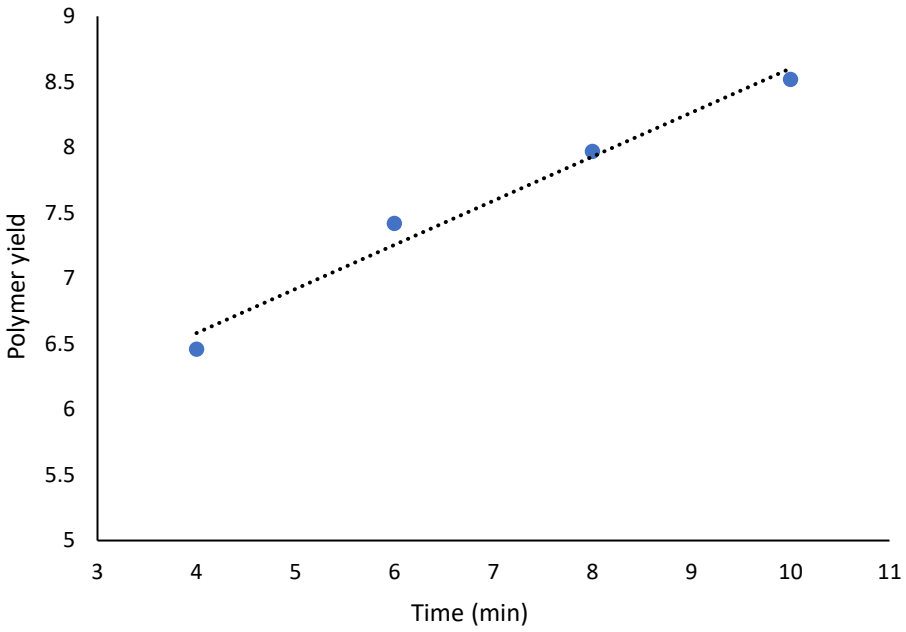

Figure 3.20 Polymer yield versus polymerization time with CGC/B/TOA.

Table 3.12 summarizes the GPC-IR results for these copolymers. The molecular weight averages increase for longer polymerizations, as expected (Figure 3.21).

Table 3.12 Molecular weight averages and SCB frequencies for ethylene/1-hexene copolymers made with CGC/B/TOA.

Run	M_w	M_n	PDI	SCB/1000C
B2-H4	88410	30980	2.85	10.8
B1-H4	95267	33644	2.83	9.5
B4-H4	89343	31430	2.84	10.1
B3-H4	87472	30884	2.83	12.1

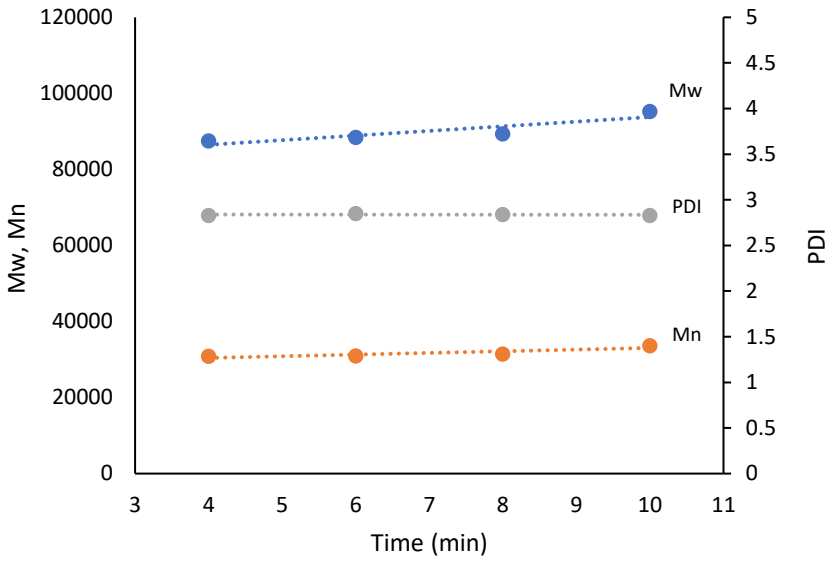

Figure 3.21 Molecular weight averages as a function of polymerization time copolymers made with CGC-Ti/B/TOA.

Figure 3.22 shows how the SCB frequency decreases with polymerization time because the concentration of 1-hexene in the reactor also decreases. Since CGC/B/TOA is a poor incorporator of 1-hexene, the comonomer drift is not as steep as for CGC/MMAO.

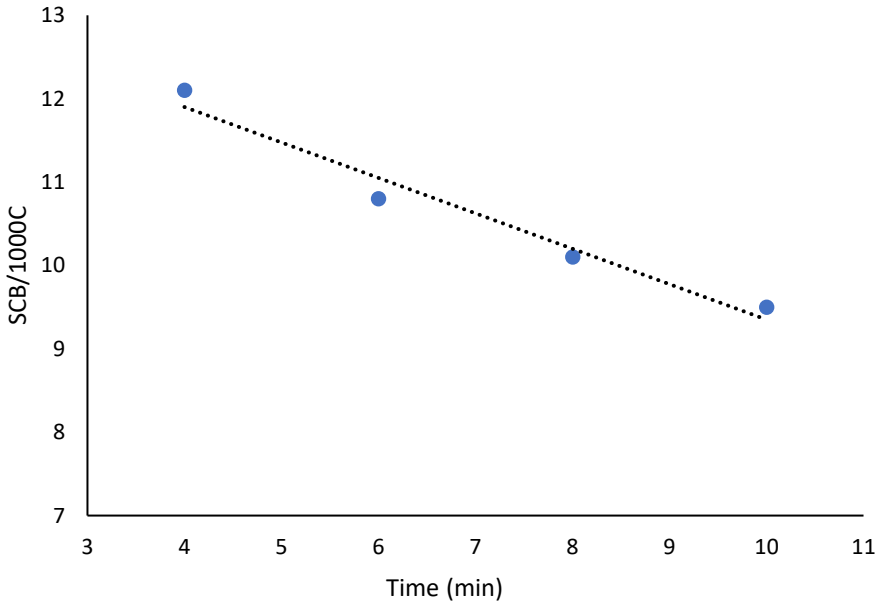

Figure 3.22 SCB frequency versus polymerization time copolymers made with CGC/B/TOA.

Figure 3.23 shows the MWDs and the average SCB frequencies measured by GPC/IR for all the samples of this set.

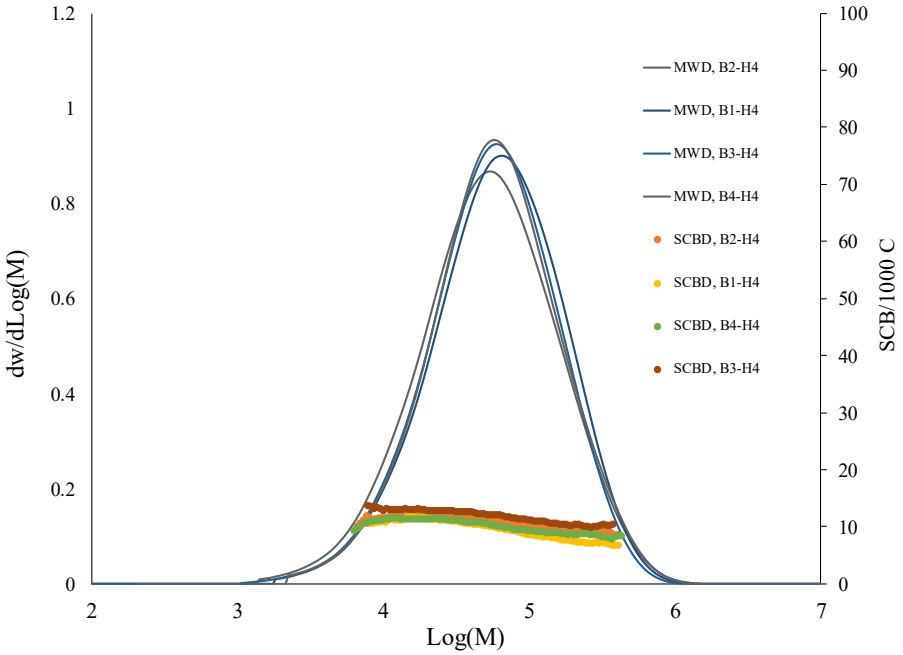

Figure 3.23 MWD and SCBD for the samples listed in Table 3.11.

3.3.2.1 Estimation of Reactivity Ratios

Table 3.13 shows the initial and final experimental results for all the samples listed in Table 3.11. The mass of unreacted comonomer varies only slightly with polymerization time, as expected from the discussion above. This slower comonomer drift is reflected in a lower 1-hexene incorporation in the copolymer, reaching only to a maximum of 2.54 mol % after four minutes of polymerization.

Table 3.13 Mass and molar balances for 1-hexene consumption at the beginning and end of polymerization with CGC/B/TOA at different times.

Run	Initial 1-Hexene (g)	Final 1-Hexene (g)	% Change in 1-Hexene mass	F_2	f_{2o} Initial	f_2 Final
B2-H4	3.955	3.474	12.162	0.0226	0.4780	0.4421
B1-H4	3.948	3.462	12.303	0.0198	0.4775	0.4412
B4-H4	3.959	3.475	12.202	0.0211	0.4782	0.4421
B3-H4	3.961	3.491	11.843	0.0254	0.4783	0.4432

Following a similar approach, the reactivity ratios were estimated as $r_1 = 72.25$, $r_2 = 0.059$, and $SSE = 6.62 \times 10^{-5}$.

3.3.3 The combined set of polymerizations

The two previous copolymerization sets (Table 3.8 and 3.11) were combined to estimate the reactivity ratios using a wider range of 1-hexene molar fractions in the copolymer, F_2, and in the liquid phase at the end of the polymerization, f_2. Table 3.14 summarizes the estimates for each set.

Table 3.14 Reactivity ratios estimates for ethylene/1-hexene copolymers made with CGC/B/TOA.

	r_1	r_2	SSE
Set 1: Varying initial 1-hexene concentrations	82.63	0.017	6.58×10^{-6}
Set 1: Varying polymerization time	72.25	0.059	6.62×10^{-5}
Set 1+2	74.57	0.0097	1.29×10^{-4}

Figure 3.24 shows that the Mayo-Lewis plots for Set 1 and Set 1+2 are similar and differ a little from that for Set 2, due to its higher estimate for r_2.

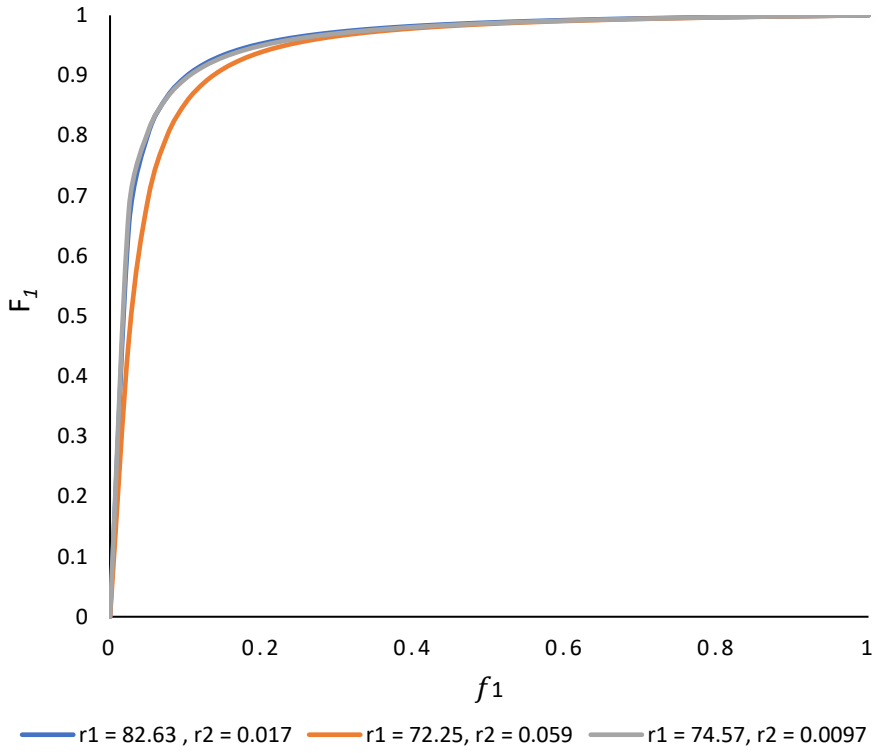

Figure 3.24 Ethylene molar fractions in the copolymer using the Mayo-Lewis equation for the three sets of reactivity ratios in Table 3.14.

3.4 Copolymerization Under Low Composition Drift with CGC/B/TOA

Five polymerizations starting with different 1-hexene concentrations were ran for only 4 minutes to compare reactivity ratio estimates with the suggested dynamic model with those of the Mayo-Lewis equation, which can only be used if the composition drift is negligible. The polymerization conditions are summarized in Table 3.15.

Table 3.15 Polymerization conditions for ethylene/1-hexene copolymerization with CGC/B/TOA under low composition drift.

Run	1-Hexene (g)	Catalyst (g)	Yield (g)
D1-H4	3.948	0.171	4.97
D1-H2	1.981	0.171	4.91
D1-H12	11.853	0.175	4.76
D1-H8	7.899	0.173	5.83
D1-H6	5.943	0.175	5.17

T = 120 °C, P_E = 120 psig, [Borate]/[CAT] = 8.40, TOA = 0.154 g, t = 4 min.

Increasing the 1-hexene reactor loading leads to a higher 1-hexene concentration in the liquid phase, as depicted in Figure 3.25.

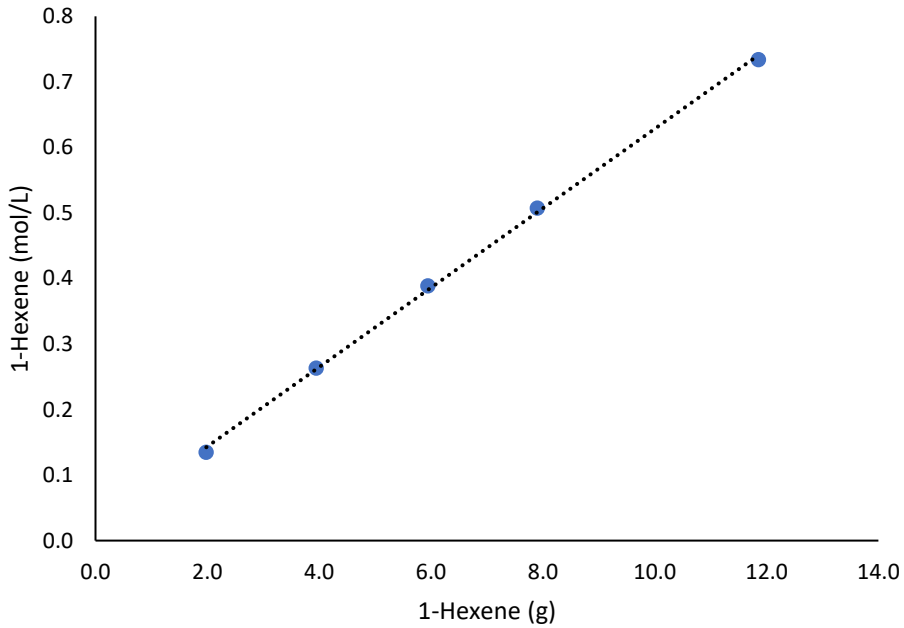

Figure 3.25 Concentration of 1-hexene in toluene versus mass of 1-hexene fed to the reactor at 120 °C

Figure 3.26 shows how the polymer yield increases with increasing 1-hexene concentration in toluene until reaching a maximum at 0.507 mol/L, after which the yield starts to decrease as 1-hexene is much less reactive than ethylene. In addition to the low reactivity of 1-hexene, some impurities transferred with higher 1-hexen concentrations could play a role in this behavior.

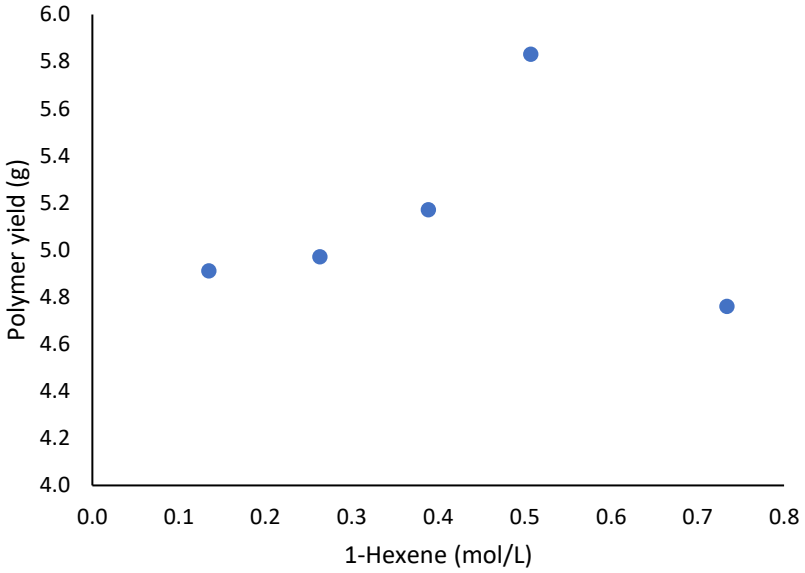

Figure 3.26 Polymer yield as a function of 1-hexene concentration for copolymerization with CGC/B/TOA under low composition drift.

As expected, the molecular weight averages decreased and the SCB frequencies increases with when more 1-hexene was added to the reactor (Table 3.16 and Figure 3.27).

Table 3.16 Molecular weight averages and SCB frequencies for ethylene/1-hexene copolymers made under low composition drift.

Run	M_w	M_n	PDI	SCB/1000C
D1-H4	120284	50791	2.37	6.86
D1-H2	145807	55960	2.61	3.59
D1-H12	74526	32652	2.28	17.5
D1-H8	86020	36790	2.34	12.7
D1-H6	105809	45247	2.34	9.80

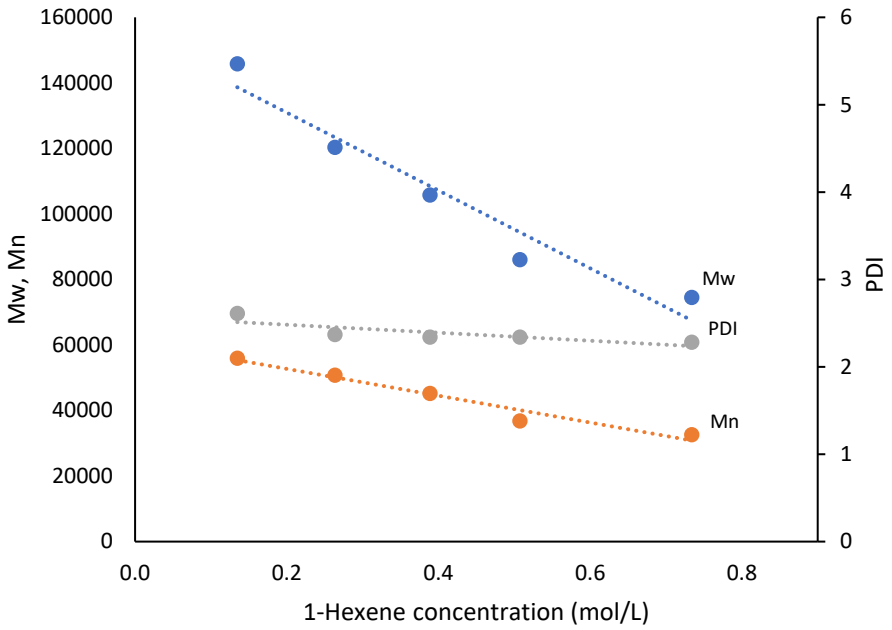

Figure 3.27 M_w, M_n, and PDI versus 1-hexene concentration for copolymers made with CGC/B/TOA under low composition drift.

Figure 3.28 shows that the SCB frequencies increase linearly with the concentration of 1-hexene concentration in toluene. The SCB distributions across the MWD are shown in Figure 3.29.

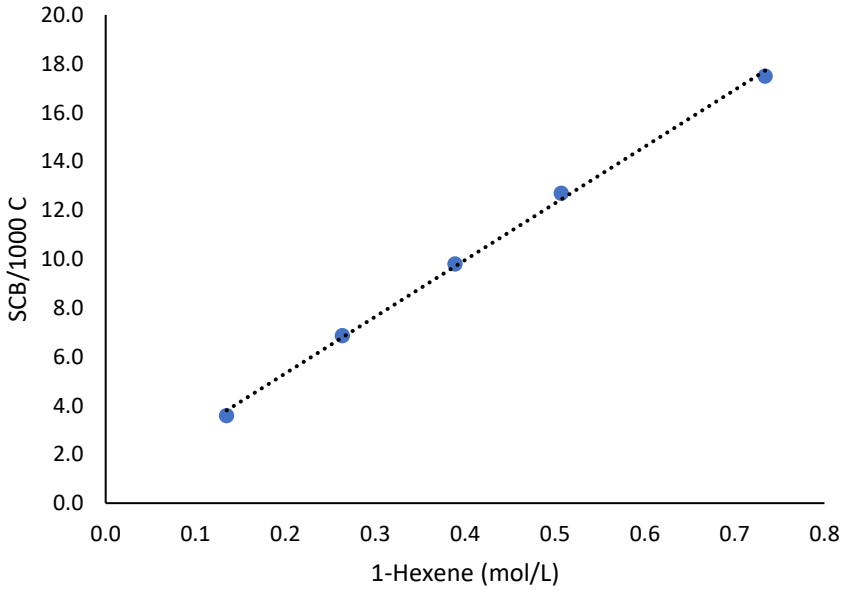

Figure 3.28 SCB frequency as a function of 1-hexene concentration for copolymers made with CGC/B/TOA under low composition drift.

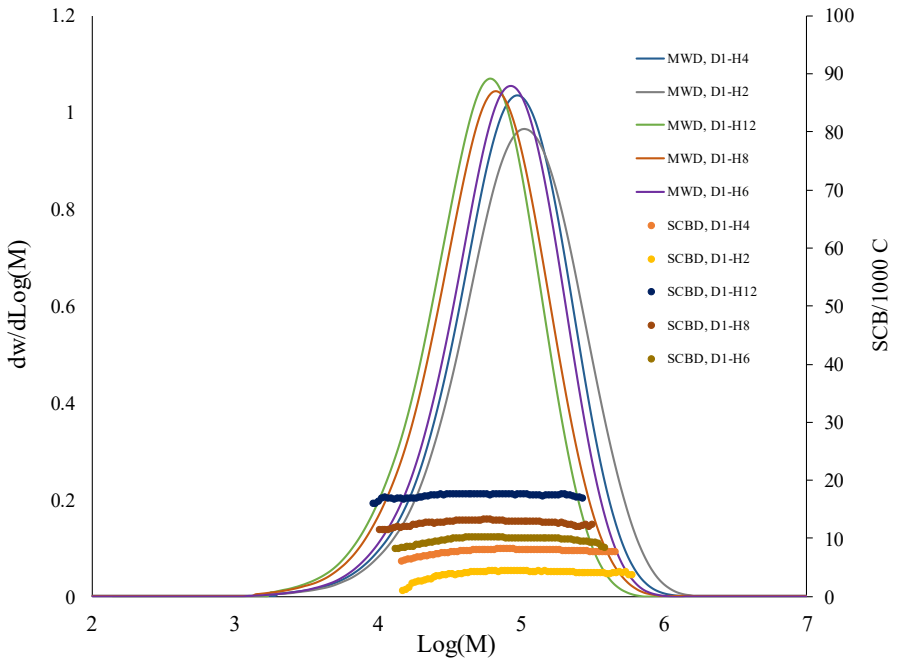

Figure 3.29 MWD and SCBD for the samples listed in Table 3.15.

3.4.1 Estimation of Reactivity Ratios

The experimental results for all samples listed in Table 3.15 are shown in Table 3.17. The composition drift for this set is low—an average of 5.11% change in 1-hexene mass—as required for the use of the Mayo-Lewis equation.

Table 3.17 Mass and molar balances for 1-hexene consumption at the beginning and end of copolymerizations with CGC/B/TOA under low composition drift.

Run	Initial 1-Hexene (g)	Final 1-Hexene (g)	% Change in 1-Hexene mass	F_2	f_{2o} Initial	f_2 Final
D1-H4	3.948	3.743	5.180	0.0141	0.4775	0.4603
D1-H2	1.981	1.875	5.352	0.0073	0.3154	0.3002
D1-H12	11.853	11.354	4.214	0.0376	0.7301	0.719
D1-H8	7.899	7.449	5.689	0.0268	0.6446	0.6279
D1-H6	5.943	5.639	5.116	0.0204	0.578	0.5616

Since the composition drift is minimal, the Mayo-Lewis equation, Eq. (3.14), could be used to estimate the reactivity ratios for this set of polymerizations using the molar fractions of 1-hexene in the copolymer, F_2, and in the reaction medium at the beginning of the reaction, f_{2_0}, listed in columns 5 and 6 of Table 3.17, respectively. The estimates were $r_1 = 65.37$, $r_2 = 0.0006$, and $SSE = 6.23 \times 10^{-7}$. Figure 3.30 plots f_{2_0} versus F_2 for these polymerizations using the estimated reactivity ratios.

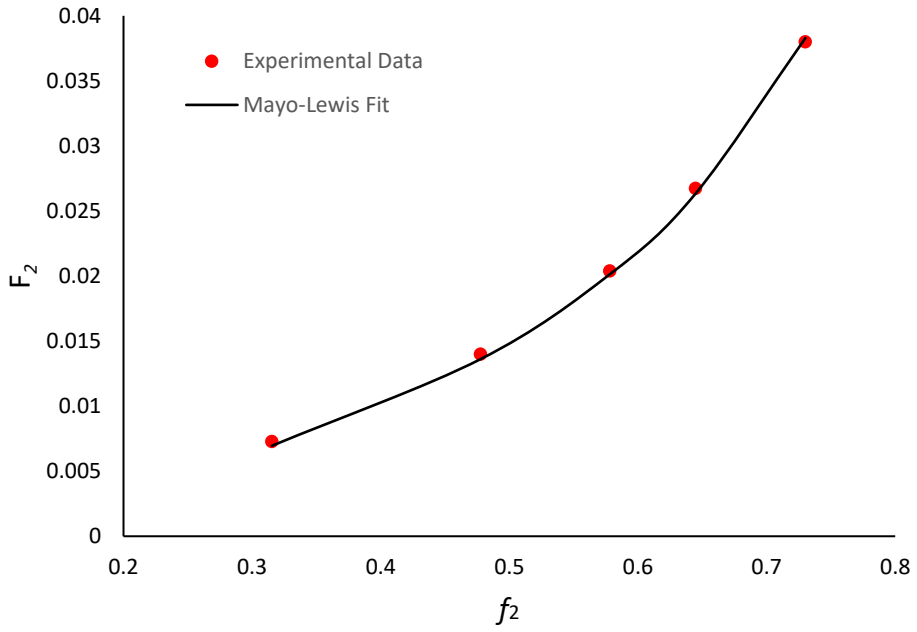

Figure 3.30 Mayo-Lewis curve fitting for copolymerizations with CGC/B/TOA under low composition drift.

The same polymerizations were used to generate a system of five ordinary differential equations applying the same mathematical treatment discussed in the previous sections. The reactivity ratios estimated with the dynamical method were $r_1 = 67.5$, $r_2 = 0.00058$, and $SSE = 9.61 \times 10^{-6}$. Figure 3.31 shows how little f_2 changes from the beginning to the end of the copolymerizations, confirming that the composition drift was negligible.

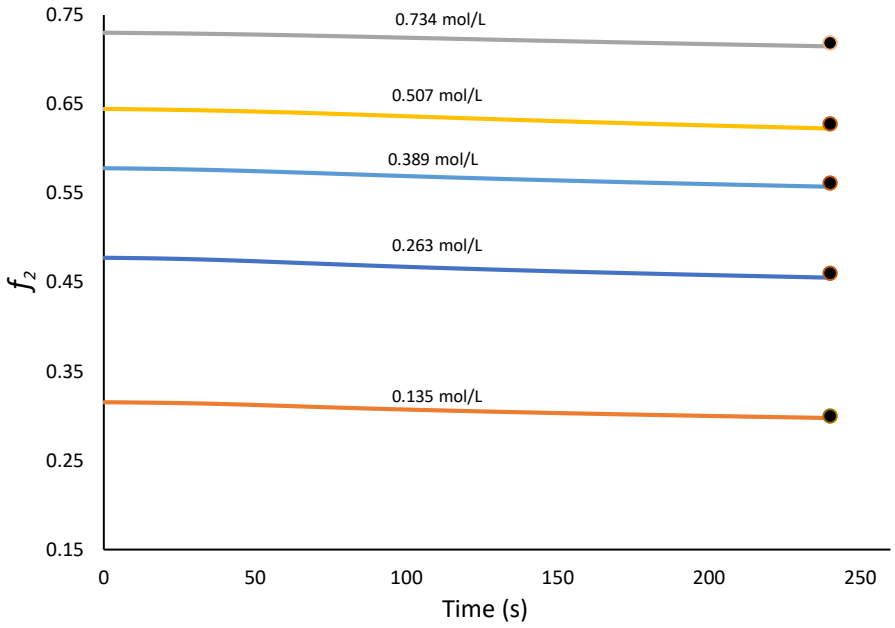

Figure 3.31 1-Hexene molar fraction drift for copolymerizations with CGC/B/TOA under negligible composition drift.

Both methods predict similar reactivity ratios, validating the performance of the suggested dynamic model as a powerful tool that can estimate these parameters at a much wider range of 1-hexene conversion. This is important because it is hard to eliminate composition drift during longer polymerizations with catalysts that have higher affinities for α-olefin comonomers, which generally applies to most copolymerizations done in lab and industrial scales.

This agreement with the Mayo-Lewis equation is depicted in Figure 3.32 for the ethylene molar fractions using reactivity ratios estimated with both methods.

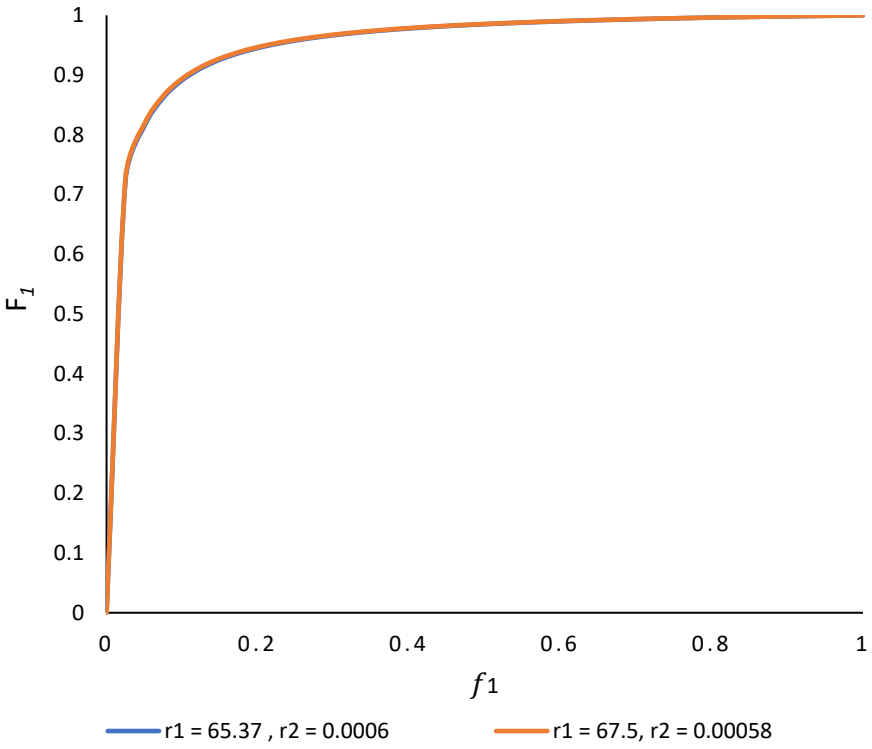

Figure 3.32 Mayo-Lewis plots with reactivity ratios estimated with the Mayo-Lewis equation and the dynamic method proposed in this thesis.

Chapter 4: A Dynamic Model to Estimate the Reactivity Ratios of Ethylene/1-Octene Copolymers

4.1 Introduction

Two sets of polymerizations were generated to determine the reactivity ratios of ethylene/1-octene copolymerization with CGC/MMAO. The first varied the initial concentrations of 1-octene in the reactor, while the second changed the polymerizations times. An extra set was also created by combining both sets.

4.2 Effect of 1-Octene Concentration

Six polymerizations were performed at different 1-octene initial concentrations from 0.1023 mol/L to 0.387 mol/L with replicated rums. The polymerization time was 15 minutes for all runs. The temperature, ethylene pressure, and cocatalyst/catalyst ratios were the same for all polymerizations (Table 4.1.). The 1-octene loadings listed in column 2 is the 1-octene mass at equilibrium, when all the polymerization conditions were satisfied and not the 1-octene mass fed into the reactor before starting the polymerization.

Table 4.1 Polymerization conditions for ethylene/1-octene copolymers made with CGC/MMAO at different 1-octene initial concentrations.

Run	1-Octene (g)	Catalyst (g)	Yield (g)
R1-O2	2.051	0.606	7.28
R1-O4	3.994	0.601	8.3
R1-O6	5.997	0.603	10.56
R1-O8	7.990	0.602	11.09
R2-O2	2.001	0.602	7.52
R2-O6	6.052	0.606	10.61

T = 120 °C, P_E = 120 psig, [MMAO]/[CAT] = 3300.85, t = 15 min.

The 1-octene concentration in the reaction medium at equilibrium depended linearly relationship on the mass of 1-octene fed to the reactor, as depicted in Figure 4.1.

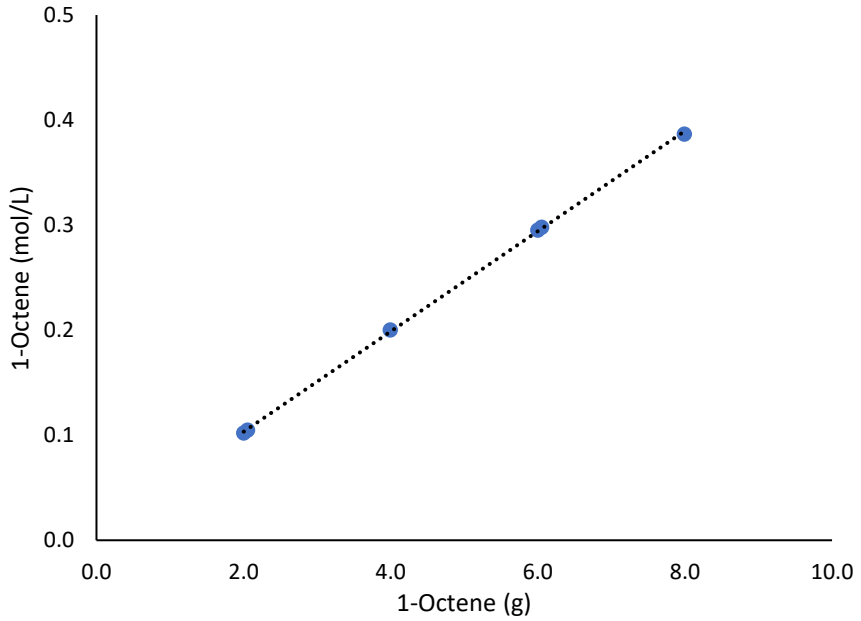

Figure 4.1 Concentration of 1-octene in toluene versus the amount of 1-octene fed to the reactor at 120 °C.

The polymer yield increased with 1-octene concentration in the liquid phase, indicating a positive effect of 1-octene on the polymerization rate (Figure 4.2). This rise in polymer yield start to decrease at higher 1-octene concentrations as 1-octene is less reactive than ethylene.

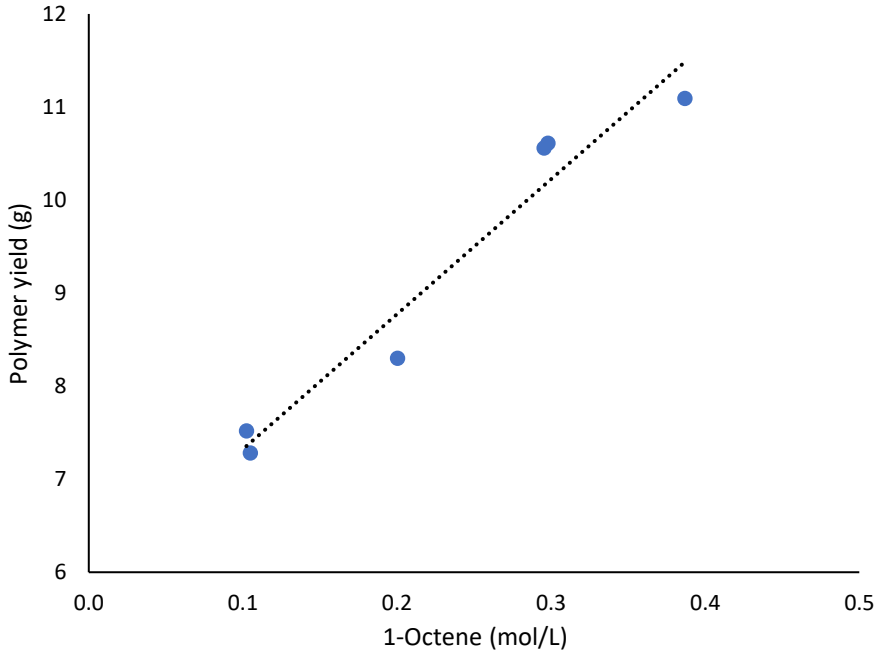

Figure 4.2 Polymer yield as a function of 1-octene concentration.

GPC/IR was used to measure the molecular weight averages and SCB frequency of these samples (Table 4.2). Figure 4.3 shows how the molecular weight averages change with 1-octene concentration in toluene. The downward trend indicates that transfer to 1-octene has a significant impact in this system.

Table 4.2 Molecular weight averages and SCB frequencies for ethylene/1-octene copolymers at different 1-octene concentrations.

Run	M_w	M_n	PDI	SCB/1000C
R1-O2	99769	39330	2.54	14.0
R1-O4	94248	38675	2.44	22.8
R1-O6	74708	30964	2.41	32.0
R1-O8	63083	26295	2.40	42.5
R2-O2	100731	40080	2.51	13.4
R2-O6	68330	28068	2.43	34.8

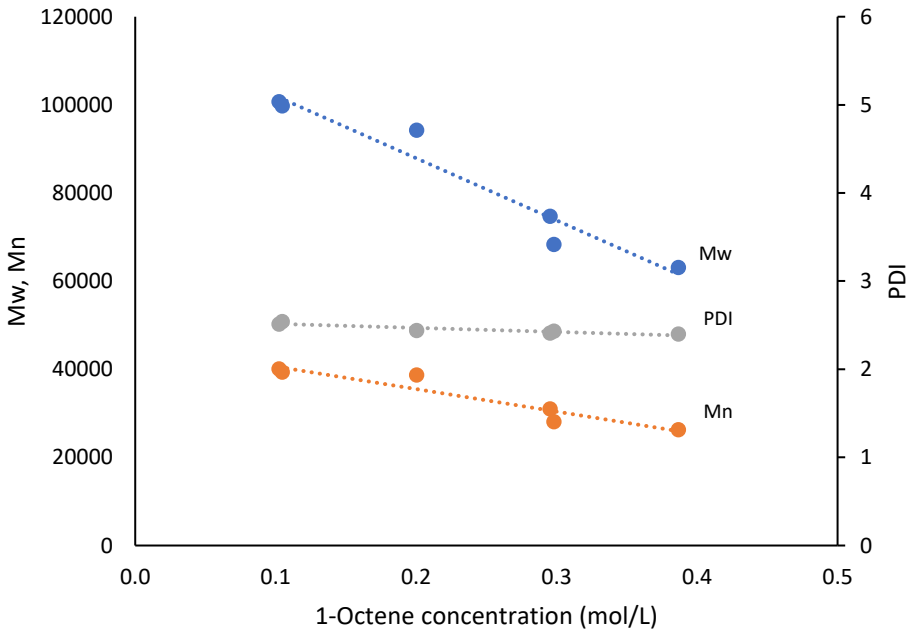

Figure 4.3 M_w, M_n, and PDI versus 1-octene concentration.

The SCB frequency in the copolymers increases with 1-octene concentration in the reactor, as shown in Figure 4.4.

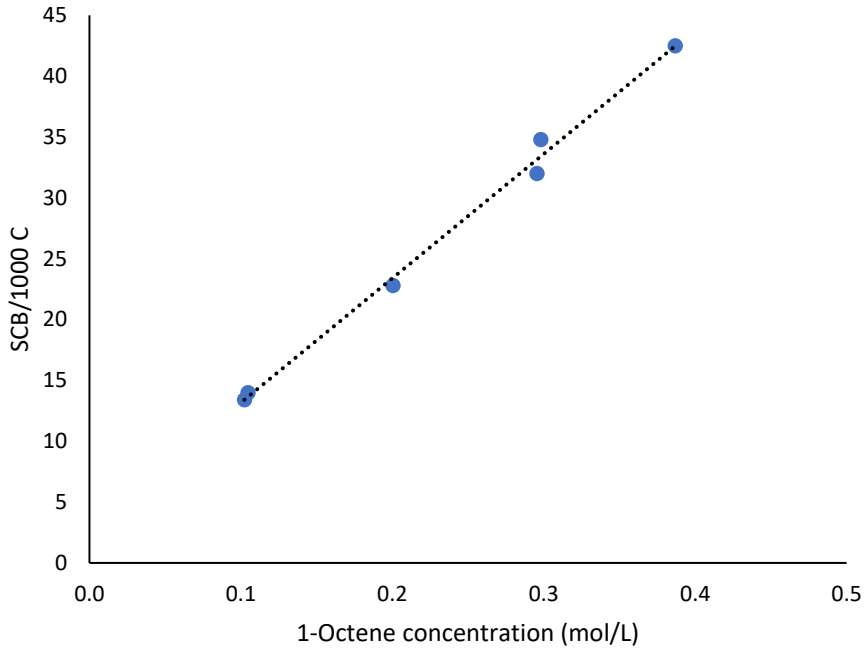

Figure 4.4 SCB frequency as a function of 1-octene concentration.

Figure 4.5 shows the SCBDs of all the samples across the MWD from the GPC/IR results.

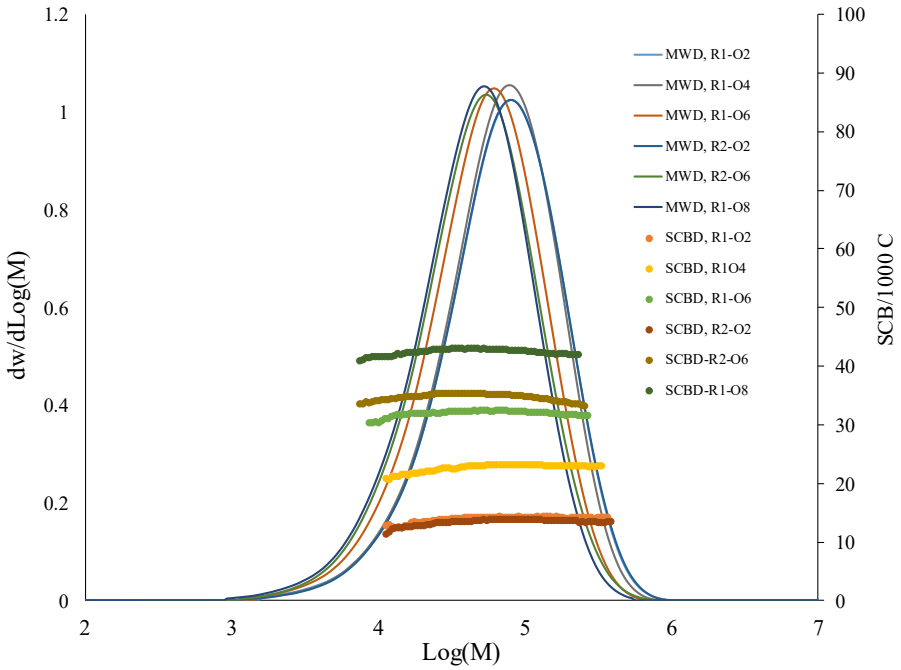

Figure 4.5 MWD and SCBD for the samples listed in Table 4.1.

4.2.1 Estimation of Reactivity Ratios

The same model derived in Chapter 3 was used to estimate the reactivity ratios of ethylene/1-octene copolymers in this chapter. Table 4.3 shows that the molar fractions of 1-octene in the copolymer, F_2, are lower than the 1-hexene fractions of Chapter 4 using the same catalytic system. The range of f_2 values, from 0.172 to 0.417, is broad enough to have a reliable estimation of reactivity ratios.

Table 4.3 Mass and molar balances for 1-octene consumption at the beginning and end of polymerization for ethylene/1-octene copolymers.

Run	Initial 1-Octene (g)	Final 1-Octene (g)	% Change in 1-Octene mass	F_2	f_{2o} Initial	f_2 Final
R1-O2	2.051	1.235	39.80	0.031	0.262	0.176
R1-O4	3.994	2.479	37.92	0.053	0.405	0.298
R1-O6	5.997	3.293	45.09	0.079	0.502	0.360
R1-O8	7.990	4.219	47.20	0.114	0.571	0.417
R2-O2	2.001	1.196	40.24	0.029	0.257	0.172
R2-O6	6.052	3.097	48.83	0.088	0.505	0.346

Eq. (3.15) was used to generate a system of six ordinary differential equations using new regression parameters. (see Appendix C). The estimated reactivity ratios were $r_1 = 16.46$ and $r_2 = 0.098$, with a sum of squared errors equal to 2.93×10^{-4}. Figure 4.6 shows how the molar fractions of 1-octene in the reactor varies as a function of time until the end of polymerization where the experimental and model values agree, as depicted in Figure 4.7.

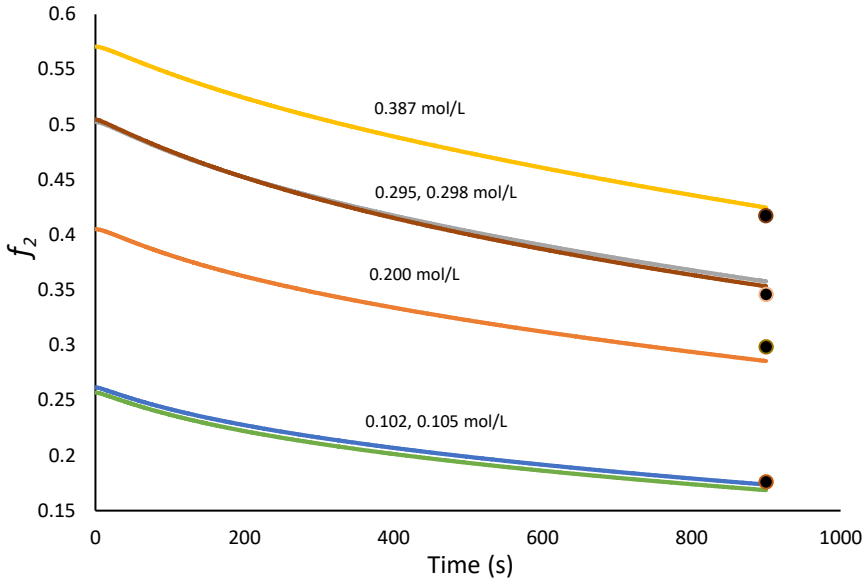

Figure 4.6 1-Octene molar fractions for ethylene/1-octene copolymerizations with CGC/MMAO as a function of time.

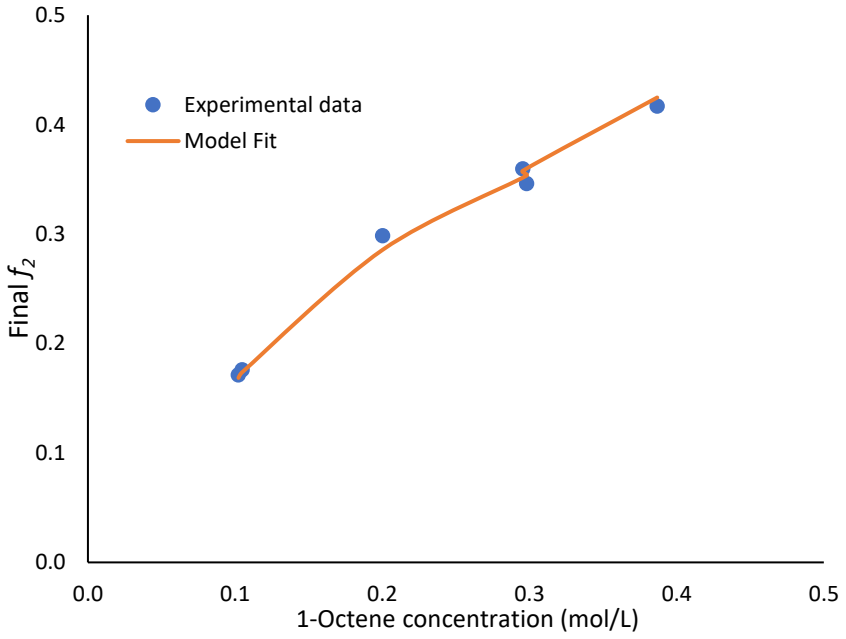

Figure 4.7 Comparison between experimental and model final f_2 values for ethylene/1-octene copolymers made with CGC/MMAO.

4.3 Effect of Polymerization Time

Four polymerizations were performed at different times and under the same 1-octene concentration to investigate the effect of time on the polymer yield, molecular weight averages, and reactivity rations. The polymerizations were performed randomly to rule out the chance of any errors caused by the well-ordered design of experiments. The temperature, ethylene pressure, cocatalyst/catalyst ratio, and 1-octene concentration were kept constant, as shown in Table 4.4.

Table 4.4 Polymerization conditions for ethylene/1-cotene copolymers at different polymerization times.

Run	Duration (min)	Catalyst (g)	Yield (g)
C3-O4	2	0.603	4.23
C2-O4	6	0.605	6.69
C4-O4	12	0.603	8.11
C1-O4	15	0.604	8.30

T = 120 °C, P_E = 120 psig, [MMAO]/[CAT] = 3300.85, 1-octene = 0.201 mol/L.

Figure 4.8 shows that the polymer yield increases with polymerization time which then tends to plateau at higher times due to the decline in catalyst activity.

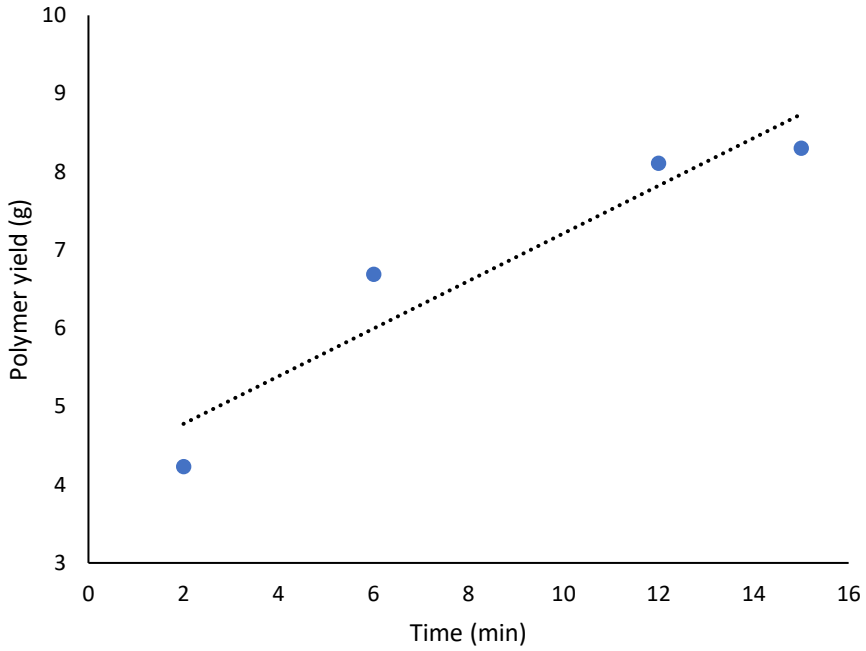

Figure 4.8 Polymer yield versus polymerization time for ethylene/1-octene copolymers made with CGC/MMAO.

Table 4.5 summarizes the GPC-IR results for these copolymers. The molecular weight averages increase for longer polymerizations, as shown in Figure 4.9. This is expected, since the concentration of 1-octene in the reactor decreases with time. This is also the reason for the drop on SCB frequency in the copolymers with polymerization time (Figure 4.10).

Table 4.5 Molecular weight averages and SCB frequencies for ethylene/1-octene copolymers at different times.

Run	M_w	M_n	PDI	SCB/1000C
C3-O4	84760	35127	2.41	26.8
C2-O4	86210	35969	2.40	23.9
C4-O4	91603	37280	2.46	23.1
C1-O4	94248	38675	2.44	22.8

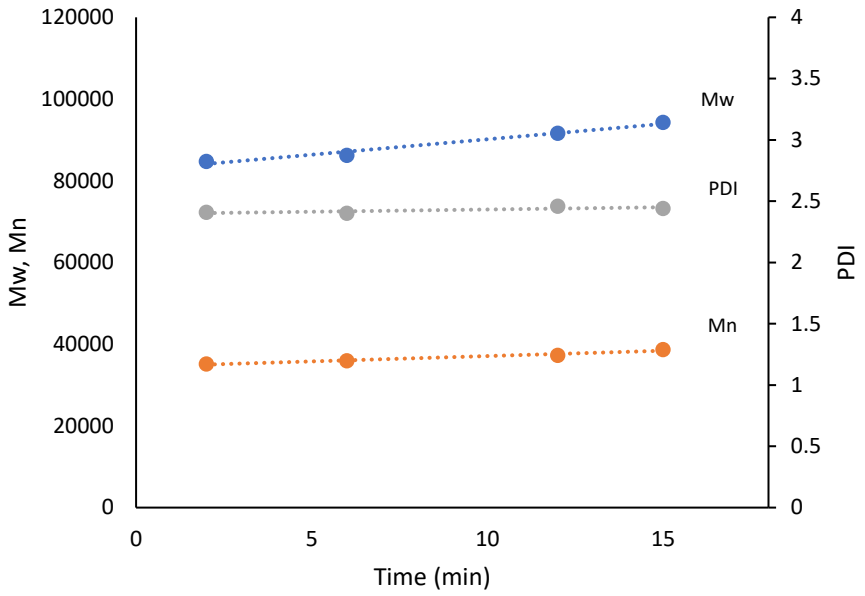

Figure 4.9 M_w, M_n, and PDI of ethylene/1-octene copolymers as a function of time.

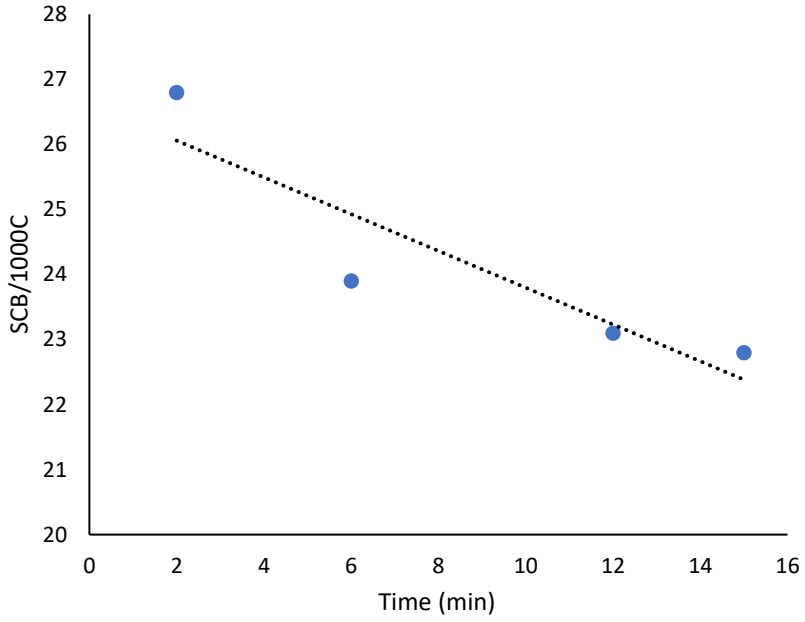

Figure 4.10 SCB frequency of ethylene/1-octene copolymers as a function of time.

Figure 4.11 shows the MWDs and average SCB frequencies across the polymer MWD measured by GPC/IR for all the samples of this set.

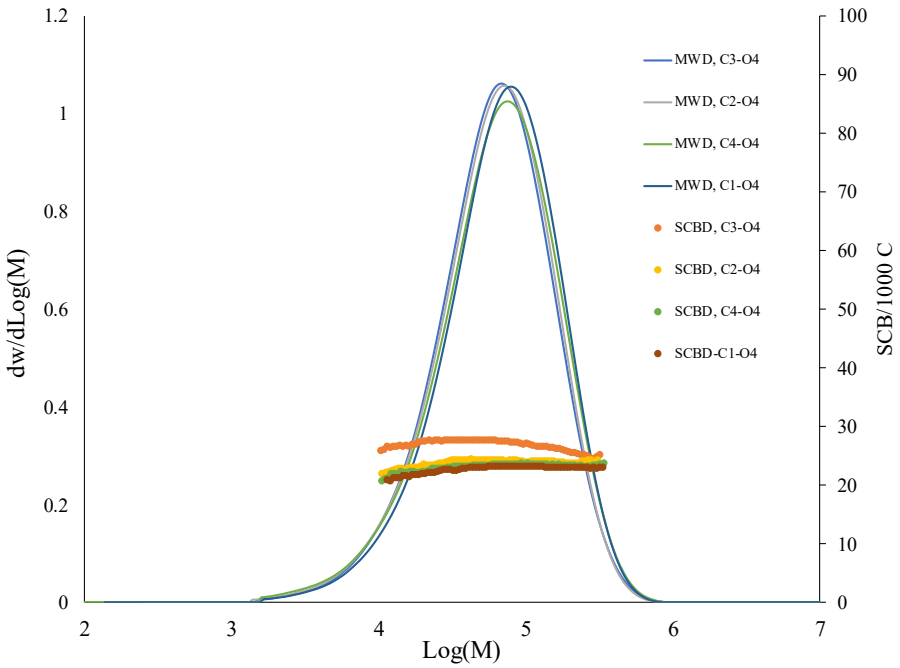

Figure 4.11 MWD and SCBD for the samples listed in Table 4.4.

4.3.1 Estimation of Reactivity Ratios

Table 4.6 summarizes the experimental results of 1-octene for all the samples listed in Table 4.4. The comonomer conversion rate increases with polymerization time, reaching a maximum of 37.92 % change in 1-octene mass.

Table 4.6 Mass and molar balances for 1-octeene consumption at the beginning and end of polymerization for ethylene/1-octene at different times.

Run	Initial 1-Octene (g)	Final 1-Octene (g)	% Change in 1-Octene mass	F_2	f_{2o} Initial	f_2 Final
C3-O4	4.014	3.108	22.55	0.0639	0.4063	0.3404
C2-O4	4.004	2.724	31.96	0.0558	0.4058	0.3326
C4-O4	4.024	2.524	37.26	0.0536	0.4069	0.3020
C1-O4	3.994	2.479	37.92	0.0528	0.4052	0.2985

Due to the high composition drift, Mayo-Lewis equation cannot be applied. The dynamic model proposed in Chapter 4 can be used to estimate the reactivity ratios. The model predictions of reactivity ratios were $r_1 = 17.62$ and $r_2 = 0.092$, with a sum of squared errors equal to 1.20×10^{-3}.

4.4 The combined set of polymerizations

Both sets were combined to create a new set that generates more ordinary differential equations and covers a wider range of f_2 and F_2 values. Table 4.7 shows the estimated values of r_1 and r_2, and the sum of squared errors for each set.

Table 4.7 Reactivity ratios estimates for ethylene/1-octene copolymers made with CGC/MMAO.

	r_1	r_2	SSE
Set 1: Varying initial 1-octene concentrations	16.46	0.098	2.93 x 10^{-4}
Set 1: Varying polymerization time	17.62	0.092	1.20 x 10^{-3}
Set 1+2	16.51	0.089	1.46 x 10^{-3}

Figure 4.12 shows that the Mayo-Lewis plots for all three sets give similar predictions of the ethylene molar fractions in the copolymer.

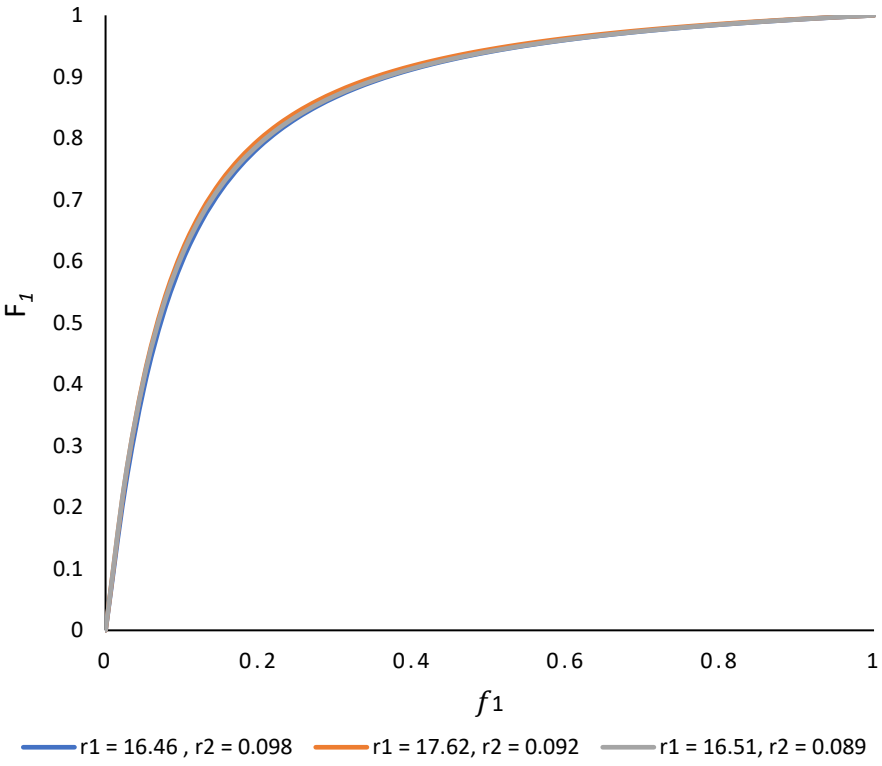

Figure 4.12 Ethylene molar fractions in the copolymer using the Mayo-Lewis equation for the three sets of reactivity ratios in Table 4.7.

Chapter 5: Conclusions and Recommendations

This dissertation investigated the microstructural characteristics of ethylene/1-hexene and ethylene/1-octene copolymers made with two catalytic systems, CGC/MMAO and CGC/B/TOA, under different polymerization conditions. For ethylene/1-hexene copolymers, four original sets of polymerizations were performed, exploring the effect of 1-hexene concentration and polymerization time on the polymer products with each catalytic system. The same was performed with ethylene/1-octene copolymers with the application of only one catalytic system, CGC/MMAO.

The main objectives of this investigation could be summarized as:

1. Explore the molecular weight measurements and SCB frequency and distribution of ethylene/1-hexene and ethylene/1-octene copolymers under different polymerization conditions.
2. Develop a dynamic mathematical model that could estimate the reactivity ratios of these copolymers of different sets
3. Assess the performance of the developed dynamic model by comparing its predictions to the Mayo-Lewis equation. For this to happen, a new set of polymerizations has to be performed at low composition drift where the Mayo-Lewis equation gives reliable estimates.
4. Compare the model reactivity ratio estimates for ethylene/1-hexene and ethylene/1-octene copolymers made with CGC/MMAO.

The molecular weight averages were found to decrease with increasing the comonomer concentration inside the reactor. The SCB frequency had the opposite behavior on both copolymer products with each catalytic system. However, the frequency was higher with CGC/MMAO than with the CGC/B/TOA.

The dynamic model gave reactivity ratio estimates for ethylene/1-hexene copolymers made with each catalytic system. The estimates of CGC/B/TOA copolymers were lower than the CGC/MMAO, showing the high activity of MMAO cocatalyst over Borate. The model's performance was found to be superior according to the results of the comparison made in Chapter

3, where the Mayo-Lewis equation and the dynamic model had a similar estimation of reactivity ratios.

The reactivity ratios estimated via the dynamic model for ethylene/1-octene copolymers made with CGC/MMAO were lower than the ethylene/1-hexene copolymers made with the same system, pointing out the higher 1-hexene incorporation tendency over 1-octene.

For future work, it is recommended to investigate the kinetics that led to a broader MWD and higher SCB frequency at the low molecular weight for the copolymers produced with CGC/B/TOA. It would also be interesting to investigate ethylene/1-octene copolymers using the same catalytic system. Another interesting research question would be the effect of other factors that impact the molecular weight averages and comonomer incorporation such as the ethylene/hydrogen ratio. Moreover, it is recommended to expand the investigation of the Mayo-Lweis equation applicability through performing several sets of polymerizations under different low composition drifts to proposed a threshold level of composition drift for the application of Mayo-Lweis equation.

References

1. Kaminsky, W. Trends in polyolefin chemistry. *Macromol Chem Phys* **209**, 459–466 (2008).

2. Soares, J. B. P. & McKenna, T. F. L. *Polyolefin Reaction Engineering*. (Wiley, 2012). doi:10.1002/9783527646944.

3. Carraher Jr., C. E. *Introduction to Polymer Chemistry*. (CRC Press, 2012). doi:10.1201/b13684.

4. Malkan, S. R. Improving the use of polyolefins in nonwovens. in *Polyolefin Fibres: Industrial and Medical Application* 288–315 (Elsevier Inc., 2009). doi:10.1533/9781845695552.2.288.

5. Manjula, B. *et al.* Use of polyolefins in hygienic applications. in *Polyolefin Fibres: Structure, Properties and Industrial Applications: Second Edition* 539–560 (Elsevier Inc., 2017). doi:10.1016/B978-0-08-101132-4.00018-7.

6. Mehdiabadi, S., Soares, J. B. P. & Brinen, J. Atypical Multiple Site Behavior of Hafnocene Catalysts in Ethylene/1-Hexene Copolymerization Using Trioctylaluminum and Borate. *Macromolecules* **51**, 7061–7076 (2018).

7. Soares, J. B. P. An overview of important microstructural distributions for polyolefin analysis. in *Macromolecular Symposia* vol. 257 1–12 (2007).

8. Deep, A., Bhatt, D., Shrivastav, V., Bhardwaj, S. K. & Malik, P. Synthesis, characterization and applications of polyolefin based eco-friendly polymer composites. in *Sustainable Polymer Composites and Nanocomposites* 65–103 (Springer International Publishing, 2019). doi:10.1007/978-3-030-05399-4_3.

9. Su, W.-F. Coordination Polymerization. in *Principles of Polymer Design and Synthesis* vol. 82 219–232 (2013).

10. Soares, J. B. P., McKenna, T. & Cheng, C. P. Coordination Polymerization. in *Polymer Reaction Engineering* (ed. Asua, J. M.) 29–117 (Blackwell Publishing Ltd, 2007). doi:10.1002/9780470692134.

11. Patel, R. M. Types and Basics of Polyethylene. in *Handbook of Industrial Polyethylene and Technology* (ed. Mark A. Spalding, A. M. C.) 105–138 (John Wiley & Sons, Inc., 2017). doi:10.1002/9781119159797.ch4.

12. Shirayama, K., Okada, T. & Kita, S.-I. *Distribution of Short-Chain Branching in Low-D ensi ty Pol yet hylene*. *JOURNAL OF POLYMER SCIENCE: PART A* vol. 3 (1965).

13. Bovey, F. A., Schilling, F. C., McCrackin, F. L. & Wagner, H. L. Short-Chain and Long-chain Branching in Low-Density Polyethylene. *Macromolecules* **9**, 76–80 (1976).

14. KULINl, L. I., Meijerink, N. L. & Starck, P. Long and short chain branching frequency in low density polyethylene (LDPE). *Pure & Applied Chemistry* **60**, 1403–1415 (1988).

15. Kissin, Y. v. Catalysts for the Manufacture of Polyethylene. in *Handbook of Industrial Polyethylene and Technology* (eds. Mark A., S. & Ananda M., C.) 25–60 (John Wiley & Sons, Inc., 2017). doi:10.1002/9781119159797.ch2.

16. Kashiwa, N. The Discovery and Progress of MgCl 2-Supported TiCl 4 Catalysts. *J Polym Sci A Polym Chem* **42**, (2004).

17. Humbert, M., Norsic, S., Raynaud, J. & Monteil, V. Activity Enhancement of MgCl2-supported Ziegler-Natta Catalysts by Lewis-acid Pre-treatment for Ethylene Polymerization. *Chinese Journal of Polymer Science* **37**, (2019).

18. Soares, J. B. P. & Pérez, O. Coordination Polymerization. in *Handbook of Polymer Synthesis, Characterization, and Processing* (eds. Enrique, S.-G. & Eduardo, V.-L.) 85–104 (John Wiley & Sons, Inc., 2013). doi:10.1002/9781118480793.ch5.

19. Long, W. P. & Breslow, D. S. Polymerization of Ethylene with Bis-(cyclopentadienyl)-titanium Dichloride and Diethylaluminum Chloride. *J Am Chem Soc* **82**, 1953–1957 (1960).

20. Soares, J. B. P. & Simon, L. C. Coordination Polymerization. in *Handbook of Polymer Reaction Engineering* (eds. T., M. & T.F., K.) 365–430 (Wiley-VCH Verlag GmbH, 2005). doi:10.1002/9783527619870.ch8.

21. Mehdiabadi, S. & Soares, J. B. P. Ethylene homopolymerization kinetics with a constrained geometry catalyst in a solution reactor. *Macromolecules* **45**, 1777–1791 (2012).

22. Mehdiabadi, S., Lhost, O., Vantomme, A. & Soares, J. B. P. Ethylene Polymerization Kinetics and Microstructure of Polyethylenes Made with Supported Metallocene Catalysts. *Ind Eng Chem Res* **60**, 9739–9754 (2021).

23. Zurek, E. & Ziegler, T. Theoretical studies of the structure and function of MAO (methylaluminoxane). *Progress in Polymer Science (Oxford)* vol. 29 107–148 Preprint at https://doi.org/10.1016/j.progpolymsci.2003.10.003 (2004).

24. Chen, E. Y. X. & Marks, T. J. Cocatalysts for metal-catalyzed olefin polymerization: Activators, activation processes, and structure-activity relationships. *Chem Rev* **100**, 1391–1434 (2000).

25. Tanaka, R., Kawahara, T., Shinto, Y., Nakayama, Y. & Shiono, T. An Alternative Method for the Preparation of Trialkylaluminum-Depleted Modified Methylaluminoxane (dMMAO). *Macromolecules* **50**, 5989–5993 (2017).

26. Mehdiabadi, S., Soares, J. B. P. & Brinen, J. Ethylene Polymerization with a Hafnocene Dichloride Catalyst Using Trioctyl Aluminum and Borate: Polymerization Kinetics and Polymer Characterization. *Macromol React Eng* **11**, (2017).

27. Bochmann, M. The chemistry of catalyst activation: The case of group 4 polymerization catalysts. *Organometallics* **29**, 4711–4740 (2010).

28. Mecking, S. & Claverie, J. P. Transition Metal-Catalyzed Polymerization in Aqueous Systems. in *Late Transition Metal Polymerization Catalysis* (eds. Rieger, B., Baugh, L. S., Kacker, S. & Striegler, S.) 231–278 (Wiley-VCH Verlag GmbH & Co. KGaA, 2005). doi:10.1002/3527601805.ch7.

29. Ittel, S. D., Johnson, L. K. & Brookhart, M. Late-metal catalysts for ethylene homo- and copolymerization. *Chem Rev* **100**, 1169–1203 (2000).

30. Soares, J. B. P. & Simon, L. C. Coordination Polymerization. in *Handbook of Polymer Reaction Engineering* (eds. Meyer, Th. & Keurentjes, J.) 365–430 (Wiley-VCH Verlag GmbH, 2005). doi:10.1002/9783527619870.ch8.

31. Xie, T., McAuley, K. B., C Hsu, J. C. & Bacon, D. W. *Gas Phase Ethylene Polymerization: Production Processes, Polymer Properties, and Reactor Modeling*. *C h e m. Res* vol. 33 (1994).

32. Mehdiabadi, S. & Soares, J. B. P. Quantifying the Copolymerization Kinetics of Ethylene and 1-Octene Catalyzed with rac-Et(Ind)2ZrCl2 in a Solution Reactor. *Macromolecules* **49**, 2448–2457 (2016).

33. POLIC, A. L., Duever, T. A. & PENLIDIS, A. Case Studies and Literature Review on the Estimation of Copolymerization Reactivity Ratios. *J Polym Sci A: Polym Chem* **36**, 813–822 (1998).

34. Mao, R. & Huglin, M. B. A new linear method to calculate monomer reactivity ratios by using high conversion copolymerization data: terminal model. *Polymer (Guildf)* **34**, 1709–1715 (1993).

35. Scott, A. J. & Penlidis, A. Computational package for copolymerization reactivity ratio estimation: Improved access to the error-in-variables-model. *Processes* **6**, (2018).

36. Behnken, D. W. Estimation of Copolymer Reactivity Ratios: An Example of Nonlinear Estimation. *JOURNAL OF POLYMER SCIENCE: PART A* **2**, 645–668 (1964).

37. Kazemi, N., Duever, T. A. & Penlidis, A. Reactivity Ratio Estimation from Cumulative Copolymer Composition Data. *Macromol React Eng* **5**, 385–403 (2011).

38. Tidwell, P. W., Mortiiz, G. A. & Er, /. *An Improved Method of Calculating Copolymerization Reactivity Ratios**. *JOURNAL OF POLYMER SCIENCE: PART A* vol. 3 (1965).

39. Kelen, T. & TÜdÕs, F. Analysis of the Linear Methods for Determining Copolymerization Reactivity Ratios. I. A New Improved Linear Graphic Method. *Journal of Macromolecular Science: Part A - Chemistry* **9**, 1–27 (1975).

40. Tüdős, F., Kelen, T., Földes-Berezsnich, T. & Turcsányi, B. Analysis of Linear Methods for Determining Copolymerization Reactivity Ratios. III. Linear Graphic Method for Evaluating Data Obtained at High Conversion Levels. *Journal of Macromolecular Science: Part A - Chemistry* **10**, 1513–1540 (1976).

41. Tidwell, P. W. & Mortimer, G. A. Science of Determining Copolymerization Reactivity Ratios. *Journal of Macromolecular Science, Part C* **4**, 281–312 (1970).

42. van der Meer, R., Linssen, H. N. & German, A. L. Improved Methods of Estimating Monomer Reactivity Ratios in Copolymerization by Considering Experimental Errors in Both Variables. *J Polym Sci A: Polym Chem* **16**, 2915–2930 (1978).

43. Patino-Lea, H., Reilly, P. M. & O'Driscoll, K. F. On the Estimation of Reactivity Rratios. *J Polym Sci : Polym Lett.* **18**, 219–227 (1980).

44. Dube, M., Sanayei, N., Penlidis, A., O'driscoll, K. F. & Reilly, P. M. A Microcomputer Program for Estimation of Copolymerization Reactivity Ratios. *J Polym Sci A: Polym Chem* **29**, 703–708 (1991).

45. Kazemi, N., Duever, T. A. & Penlidis, A. Design of experiments for reactivity ratio estimation in multicomponent polymerizations using the error-in-variables approach. *Macromol Theory Simul* **22**, 261–272 (2013).

46. Kazemi, N., Duever, T. A. & Penlidis, A. A powerful estimation scheme with the error-in-variables-model for nonlinear cases: Reactivity ratio estimation examples. *Comput Chem Eng* **48**, 200–208 (2013).

47. Kazemi, N., Lessard, B. H., Marić, M., Duever, T. A. & Penlidis, A. Reactivity ratio estimation in radical copolymerization: From preliminary estimates to optimal design of experiments. *Ind Eng Chem Res* **53**, 7305–7312 (2014).

48. Habibi, A., Vasheghani-Farahani, E., Semsarzadeh, M. A. & Sadaghiani, K. A Generalized Least Square Model for the Determination of Monomer Reactivity Ratios in Free Radical Copolymerization Systems. *Macromol. Theory Simul.* **12**, 184–195 (2003).

49. Ashenagar, S., Ziaee, F. & Shabani, I. Reactivity ratio determination of styrene and 2-ethylhexyl acrylate by least squares methods. *International Journal of Plastics Technology* **19**, 191–198 (2015).

50. Uozumi, T. & Soga, K. Copolymerization of olefins with Kaminsky-Sinn-type cat a1 y s t s. *Makromol. Chem* **193**, 823–831 (1992).

51. Al-Saleh, M. A., Soares, J. B. P. & Duever, T. A. The integrated deconvolution estimation model: A parameter estimation method for ethylene/α-Olefin Copolymers Made with Multiple-Site Catalysts. *Macromol React Eng* **4**, 578–590 (2010).

52. Beckingham, B. S., Sanoja, G. E. & Lynd, N. A. Simple and Accurate Determination of Reactivity Ratios Using a Nonterminal Model of Chain Copolymerization. *Macromolecules* **48**, 6922–6930 (2015).

53. Lynd, N. A., Ferrier, R. C. & Beckingham, B. S. Recommendation for Accurate Experimental Determination of Reactivity Ratios in Chain Copolymerization. *Macromolecules* **52**, 2277–2285 (2019).

54. Mehdiabadi, S., Lhost, O., Vantomme, A. & Soares, J. B. P. Ethylene/1-Hexene Copolymerization Kinetics and Microstructure of Copolymers Made with a Supported Metallocene Catalyst. *Macromol. React. Eng.* **15**, (2021).

55. Rudin, A. & Choi, P. Practical Aspects of Molecular Weight Measurements. in *The Elements of Polymer Science & Engineering* vol. 3 73–120 (2013).

56. Nguyen, T. Q. & Kausch, H. H. Molecular Weight Distribution — Characterisation by GPC. in *Mechanical Properties and Testing of Polymers. Polymer Science and Technology Series* (ed. Swallowe, G. M.) vol. 3 151–155 (Springer, 1999).

57. Grubisic, Z., Rempp, P. & Benoit, H. A universal calibration for gel permeation chromatography. *Journal of Polymer Science Part C: Polymer Letters* **5**, 735–759 (1967).

58. Shiraymia, K., Kita, S.-I. & Watabe, H. Effects of Branching on some Properties of Ethylene/a-Olefin Copolymers. *Macromol Chem Phys* **151**, 97–120 (1972).

59. Blitz, J. P. & Mcfaddln, D. C. The Characterization of Short Chain Branching in Polyethylene Using Fourier Transform Infrared Spectroscopy. *J Appl Polym Sci* **51**, 13–20 (1994).

60. Deslauriers, P. J., Rohlfing, D. C. & Hsieh, E. T. Quantifying short chain branching microstructures in ethylene 1-olefin copolymers using size exclusion chromatography and Fourier transform infrared spectroscopy (SEC-FTIR). *Polymer (Guildf)* **43**, 159–170 (2002).

61. Tribe, K., Saunders, G. & Meißner, R. Characterization of Branched Polyolefins by High Temperature GPC Utilizing Function Specific Detectors. *Macromol Symp* **236**, 228–234 (2006).

62. Palacios, A. Polymerization Kinetics and Structure-Property Relationships of Ethylene/1-Hexene Copolymers. (2018). doi:10.7939/R30000G3K.

Appendix A: Regression Parameters for Ethylene/1-Hexene copolymerization with CGC/MMAO

Table A.1 Regression estimates for ethylene/1-hexene copolymers made with CGC/MMAO at different 1-hexene concentrations.

ID	p_1	p_2	p_3	q_1	q_2	SSE	R^2
R1-H4	0.002	6.076	-0.531	265.7	365.2	1.41×10^{-3}	0.943
R1-H8	0.004	6.914	-0.486	321.1	485.1	8.40×10^{-4}	0.948
R1-H10	0.006	4.192	-0.160	262.4	365	7.00×10^{-4}	0.883
R2-H4	0.002	5.877	-2.279	210.8	588.5	6.48×10^{-4}	0.981
R2-H2	0.003	3.488	-1.402	111.6	406.1	6.25×10^{-4}	0.982
R1-H2	0.002	4.185	-0.611	132.8	280	2.28×10^{-3}	0.951

Table A.2 Regression estimates for ethylene/1-hexene copolymers made with CGC/MMAO at different polymerization times.

ID	p_1	p_2	p_3	q_1	q_2	SSE	R^2
R1-H6	0.004	5.310	-2.343	196.5	1297	3.38×10^{-4}	0.967
R2-H6	0.007	1.939	-0.058	70.71	998.1	2.98×10^{-4}	0.943
R3-H6	0.008	1.357	-0.228	36.94	706.8	2.90×10^{-4}	0.911
R4-H6	0.007	3.299	-1.787	107.5	864.7	3.74×10^{-4}	0.944

Appendix B: Regression Parameters for Ethylene/1-Hexene copolymerization with CGC/B/TOA

Table B.1 Regression estimates for ethylene/1-hexene copolymers made with CGC/B/TOA at different 1-hexene concentrations.

ID	p_1	p_2	p_3	q_1	q_2	SSE	R^2
B1-H4	-0.00100	4.635	-15.28	-11.63	4263	2.42×10^{-3}	0.976
B1-H6	0.00113	3.198	-9.466	-37.47	3009	1.97×10^{-3}	0.985
B1-H2	0.00154	2.494	-3.397	-14.01	1096	3.69×10^{-3}	0.974
B1-H8	-0.00003	3.514	-10.35	-46.03	3581	2.50×10^{-3}	0.984
B2-H2	0.00199	2.140	-3.625	-27.77	1342	3.28×10^{-3}	0.976

Table B.2 Regression estimates for ethylene/1-hexene copolymers made with CGC/B/TOA at different polymerization times.

ID	p_1	p_2	p_3	q_1	q_2	SSE	R^2
B2-H4	0.001	4.025	-12.86	-31.43	4670	2.09×10^{-3}	0.962
B1-H4	-0.001	4.635	-15.28	-11.63	4263	2.42×10^{-3}	0.976
B4-H4	0.006	2.326	-6.622	-22.81	1524	2.01×10^{-3}	0.957
B3-H4	-0.005	6.299	-23.51	-4.42	5554	2.91×10^{-3}	0.970

Table B.3 Regression estimates for ethylene/1-hexene copolymers made with CGC/B/TOA at low composition drift.

ID	p_1	p_2	p_3	q_1	q_2	SSE	R^2
D1-H4	0.005	1.466	-1.99	-65.88	3393	1.03×10^{-3}	0.968
D1-H2	0.007	0.59	0.595	-79.15	2960	1.25×10^{-3}	0.961
D1-H12	0.007	1.454	12.4	-86.53	8076	5.48×10^{-4}	0.967
D1-H8	0.005	2.145	5.82	-98.27	8506	9.99×10^{-4}	0.965
D1-H6	0.005	1.392	2.738	-75.07	4691	8.79×10^{-4}	0.96

Appendix C: Regression Parameters for Ethylene/1-Octene copolymerization with CGC/MMAO

Table C.1 Regression estimates for ethylene/1-octene copolymers made with CGC/MMAO at different 1-octene concentrations.

ID	p_1	p_2	p_3	q_1	q_2	SSE	R^2
R1-O2	0.004	3.772	-1.161	130.2	319.6	5.48×10^{-4}	0.982
R1-O4	0.004	3.510	-1.649	111.8	842.3	5.59×10^{-4}	0.976
R1-O6	0.004	4.413	-2.275	135.4	956.5	7.56×10^{-4}	0.976
R1-O8	0.005	4.196	-2.144	147.5	1191	6.09×10^{-4}	0.971
R2-O2	0.003	3.859	-1.302	123.2	453.9	7.07×10^{-4}	0.980
R2-O6	0.003	6.371	-1.872	230.9	580.4	6.96×10^{-4}	0.978

Table C.2 Regression estimates for ethylene/1-octene copolymers made with CGC/MMAO at different polymerization times.

ID	p_1	p_2	p_3	q_1	q_2	SSE	R^2
C3-O4	0.019	-0.049	0.125	-7.755	41.22	1.61×10^{-4}	0.944
C2-O4	-0.001	7.015	-0.125	245.0	328.6	1.96×10^{-4}	0.985
C4-O4	0.002	6.092	-0.387	212.8	512.5	2.83×10^{-4}	0.990
C1-O4	0.004	3.510	-1.649	111.8	842.3	5.59×10^{-4}	0.976